



Rotenone Induces a Neuropathological Phenotype in Cholinergic-like Neurons Resembling Parkinson's Disease Dementia (PDD)

Daniela Giraldo-Berrio¹ · Miguel Mendivil-Perez¹ · Carlos Velez-Pardo¹ · Marlene Jimenez-Del-Rio¹

Received: 16 November 2023 / Revised: 12 April 2024 / Accepted: 1 May 2024 / Published online: 6 June 2024
© The Author(s) 2024

Abstract

Parkinson's disease with dementia (PDD) is a neurological disorder that clinically and neuropathologically overlaps with Parkinson's disease (PD) and Alzheimer's disease (AD). Although it is assumed that alpha-synuclein (α -Syn), amyloid beta ($A\beta$), and the protein Tau might synergistically induce cholinergic neuronal degeneration, presently the pathological mechanism of PDD remains unclear. Therefore, it is essential to delve into the cellular and molecular aspects of this neurological entity to identify potential targets for prevention and treatment strategies. Cholinergic-like neurons (ChLNs) were exposed to rotenone (ROT, 10 μ M) for 24 h. ROT provokes loss of $\Delta\Psi_m$, generation of reactive oxygen species (ROS), phosphorylation of leucine-rich repeated kinase 2 (LRRK2 at Ser⁹³⁵) concomitantly with phosphorylation of α -synuclein (α -Syn, Ser¹²⁹), induces accumulation of intracellular $A\beta$ (i $A\beta$), oxidized DJ-1 (Cys¹⁰⁶), as well as phosphorylation of TAU (Ser²⁰²/Thr²⁰⁵), increases the phosphorylation of c-JUN (Ser⁶³/Ser⁷³), and increases expression of proapoptotic proteins TP53, PUMA, and cleaved caspase 3 (CC3) in ChLNs. These neuropathological features resemble those reproduced in presenilin 1 (PSEN1) E280A ChLNs. Interestingly, anti-oxidant and anti-amyloid cannabidiol (CBD), JNK inhibitor SP600125 (SP), TP53 inhibitor pifithrin- α (PFT), and LRRK2 kinase inhibitor PF-06447475 (PF475) significantly diminish ROT-induced oxidative stress (OS), proteinaceous, and cell death markers in ChLNs compared to naïve ChLNs. In conclusion, ROT induces p- α -Syn, i $A\beta$, p-Tau, and cell death in ChLNs, recapitulating the neuropathology findings in PDD. Our report provides an excellent in vitro model to test for potential therapeutic strategies against PDD. Our data suggest that ROT induces a neuropathologic phenotype in ChLNs similar to that caused by the mutation PSEN1 E280A.

Keywords Alzheimer's disease · Alpha-synuclein · E280A · Parkinson · Presenilin · Mutation · Rotenone

Introduction

Parkinson's disease (PD) is a progressive chronic neurologic disorder clinically characterized by slowing of movements in the limbs, face, walking or overall body (bradykinesia), resting tremor which typically stops when the patient is active or moving, rigidity or stiffness in the arms, legs or trunk

(Jankovic 2008; Bloem et al. 2021). Alzheimer's disease (AD) is also a common progressive disorder beginning with mild memory loss leading to typical features of dementia such as severe impairments in thought, memory, and language (Knopman et al. 2021). While PD is the consequence of dramatic loss of dopaminergic (DAergic) neurons in the ventral part of the pars compacta in the substantia nigra and deficit of dopaminergic innervation of striatum (Dickson 2012), AD is caused by the losses of forebrain cholinergic neurons of the nucleus basalis of Meynert (Ch4) and cholinergic projection from the Medial septum nucleus (Ch1) to hippocampus (Liu et al. 2015; Pepeu and Grazia Giovannini 2017). Intriguingly, Parkinson's disease with dementia (PDD) is a neurological disorder that overlaps with PD and AD (Irwin et al. 2013). By definition, PDD is a clinical condition wherein patients with diagnosis of PD goes together with cognitive dysfunction (e.g., deficits in attention, executive functioning, visuospatial processing), neuropsychiatric

✉ Carlos Velez-Pardo
calberto.velez@udea.edu.co

✉ Marlene Jimenez-Del-Rio
marlene.jimenez@udea.edu.co

Miguel Mendivil-Perez
miguel.mendivil@udea.edu.co

¹ Neuroscience Research Group, Medical Research Institute, Faculty of Medicine, University of Antioquia (UdeA), Calle 70 No. 52-21, and Calle 62 # 52-59, Building 1, Room 412, Medellin, Antioquia, Colombia

symptoms (e.g., hallucinations, depression), memory loss and dementia (Goetz et al. 2009; Vasconcellos and Pereira 2015; Phillips et al. 2023). Pathologically, PDD is characterized by severe burden of Lewy bodies, which are composed of the pathological PD-associated protein α -synuclein (α -Syn) and Lewy neurites, as well as extensive diffuse amyloid- β -reactive plaque pathology, Tau-reactive diffuse threads and neurofibrillary tangles (NFT), which are AD-associated pathological markers (Smith et al. 2019; Kouli et al. 2020). Although it is supposed that α -Syn, A β , and Tau might synergistically induce cholinergic and DAergic neuronal degeneration (Kim 2023), presently the pathological mechanism of PDD remains unclear. Therefore, it is essential to delve into the cellular and molecular aspects of this neurological entity to identify potential targets for the prevention and treatment strategies (Han et al. 2021).

Rotenone (ROT, PubChem CID 6758), a naturally occurring organic compound found in the roots of the *Derris* (Sae-Yun et al. 2006; Zubairi et al. 2014) and *Lonchocarpus* (Fang and Casida 1999) plant species, is used worldwide due to its broad spectrum insecticidal (Zhang et al. 2022a), acaricidal and pesticide properties (<http://www.chm.bris.ac.uk/motm/rotenone/>; available in November, 2023). Importantly, ROT induces specific degeneration of DAergic neurons in vitro and in vivo (Lawana and Cannon 2020), which intrinsically deteriorate in PD (Giguère et al. 2018). Mechanistically, ROT acts as a strong inhibitor of complex I of the mitochondrial respiratory chain (Read et al. 2021) via inhibition of electron transfer from the iron-sulfur centers in complex I to ubiquinone, leading to a blockade of the I_Q site (Schiller and Zickermann 2022), and over-reduction of complex I causes electrons to leak and produce reactive oxygen species (ROS) such as superoxide anion radical (O₂⁻). This radical can dismutate into non-radical reactive hydrogen peroxide, H₂O₂ (Li et al. 2003; Mailloux 2015). In turn, this last compound, via signaling mechanisms (Marinho et al. 2014; Antunes and Brito 2017), induces regulated cell death apoptosis (Velez-Pardo and Jimenez-Del-Rio 2020). Although, the effect of ROT appears tissue-specific, it has also been demonstrated that ROT induces cell death of non-catecholaminergic neurons such as cholinergic neurons (ChNs) in an organotypic co-culture brain slice model (Ullrich and Humpel 2009). This last observation suggests that hippocampal Lewy pathology might be associated with cholinergic degeneration in PD with cognitive decline (Liu et al. 2019; Aarsland et al. 2021). These may explain why some brains from PDD patients present AD features such as A β plaques and tau containing NFT (Irwin et al. 2013; Jellinger 2023). These observations suggest that α -Syn, A β , and Tau might together induce neuronal degeneration. In line with this view, it has been shown that ROT induced α -Syn and A β aggregation, as well as increased hyperphosphorylation of Tau in cultured cells from hippocampus, locus coeruleus and substantia nigra of newborn Lewis rats (Chaves et al. 2010). Moreover, ROT

triggered a cerebral tauopathy in rats (Höglinger et al. 2005). However, the mechanism by which ROT induce co-existence of α -Syn, A β , and Tau is unknown. Furthermore, the mechanism by which ROT produces proteinopathy in cholinergic neurons is yet unknown. Although ROT has extensively been used as model neurotoxin to disclose the molecular events of PD (Ke et al. 2021), currently there are not in vitro model of PDD available.

Mesenchymal stromal cells (MSCs) derived from umbilical cord Warton's Jelly (UC-WJ) are multipotent cells that have the potential to differentiate into neuroectodermal cell lineage (Dominici et al. 2006; Viswanathan et al. 2019). Our laboratory has used WJ-MSCs to recapitulate the neuropathological features of familial AD (FAD) due to a mutation in presenilin 1 (PSEN1) E280A (Soto-Mercado et al. 2020). Indeed, cultured MSCs bearing the wild-type (WT) and variant PSEN1 E280A in *Cholinergic-N-Run* medium (Mendivil-Perez et al. 2019) transdifferentiated into cholinergic-like neurons (ChLNs). Notably, PSEN1 E280A ChLNs but not WT PSEN1 ChLNs showed accumulation of intracellular amyloid precursor protein fragments (iAPP β /iA β), and displayed phosphorylation of protein TAU (p-TAU at residues Ser²⁰²/Thr²⁰⁵). Also, the variant ChLNs E280A presented oxidation of stress sensor DJ-1Cys¹⁰⁶-SH into DJ-1Cys¹⁰⁶-SO₃, phosphorylation of c-JUN at Ser⁶³/Ser⁷³, and detection of dichlorofluorescein (DCF)-positive cells as evidenced of generation of ROS such as H₂O₂, oxidative stress (OS), concomitant loss of the $\Delta\Psi$ m, DNA fragmentation, and Ca²⁺ flux dysregulation (Soto-Mercado et al. 2020). Despite these advances, no chemical neurotoxin-induced model of FAD has yet been revealed.

Given that PDD appears neuropathologically to recapitulate AD and PD, we hypothesize that ROT can replicate both FAD and PD cellular hallmarks in ChLNs, which represent an excellent model to study PDD. We have treated ChLNs derived from WJ-MSCs with ROT (1, 5, 10 μ M) for 24 h. For comparative and validation purposes, we used WJ-MSC-derived PSEN1 E280A ChLNs. We found that (i) ROT induces generation of ROS and H₂O₂, loss of $\Delta\Psi$ m, oxidized DJ-1, accumulation of iA β , p-Ser²⁰²/Thr²⁰⁵ TAU, and cell death happens in ChLNs, as it appears in PSEN1 E280A ChLNs FAD; (ii) ROT induces concomitant p-Ser⁹³⁵ LRRK2 and p-Ser¹²⁹- α -Syn in ChLNs. Outstandingly, we report for the first time that p-LRRK2 and p- α -Syn also endogenously appear in PSEN1 E280A ChLNs; (iii) ROT increases the phosphorylation of c-JUN at residues Ser⁶³/Ser⁷³ and the expression of TP53, PUMA and pro-apoptotic marker cleaved caspase 3 (CC3) in ChLNs. A similar profile of positive protein markers was also observed in PSEN1 E280A ChLNs; (iv) ROT impairs ACh-induced transient Ca²⁺ influx in ChLNs to a similar extend as observed in PSEN1 E280A ChLNs. Interestingly, ChLNs co-treated with ROT and anti-amyloidogenic and antioxidant cannabidiol, JNK

inhibitor SP600125, and LRRK2 inhibitor PF-06447475 significantly blunted A β , oxDJ-1, p- α -Syn, p-TAU, and CC3, respectively. Given that ROT and iA β trigger mitochondrial dysfunction, and produce H₂O₂, they may be an important etiopathogenic factor involved not only in AD and PD (Velez-Pardo and Jimenez-Del-Rio 2020) but also in PDD. Therefore, mitochondria, LRRK2, and H₂O₂ might be targets for therapeutic treatment for PDD (Macdonald et al. 2018; Abrishamdar et al. 2023).

Materials and Methods

Transdifferentiation of Mesenchymal Stromal Cell into Cholinergic-like Neurons

ChLN differentiation was performed according to (Mendivil-Perez et al. 2019). Briefly, the WT (TBC# WJMISC-19) and PSEN1 E280A (TBC# WJMISC-24) were obtained from the Neuroscience Tissue Bank-UdeA. MSCs were seeded at $1\text{--}1.5 \times 10^4$ cells/cm² in laminin-treated culture plates for 24 h in regular culture medium (RCm). The medium was removed, and cells were incubated in cholinergic differentiation medium (*Cholinergic-N-Run* medium, hereafter *Ch-N-Rm*) containing DMEM/F-12 media 1:1 Nutrient Mixture (Gibco cat# 10,565,018; 1204 N Western St, Suite C, Amarillo, TX, USA), 10 ng/mL basic fibroblast growth factor (bFGF) recombinant human protein (Gibco Cat# 13,256,029), 50 μ g/mL sodium heparin (Hep, Sigma-Aldrich cat# H3393; 3050 Spruce Street, St. Louis, MO 63103, USA), 0.5 μ M all-trans retinoic acid, 50 ng/mL sonic hedgehog peptide (SHH, Sigma cat# SRP3156) and 1% FBS at 37 °C for 7 days. After this process of transdifferentiation, the cells were labeled as WT PSEN1 or PSEN1 E280A ChLNs. Since *Ch-N-Rm* contains several factors (e.g., growth factors) that might interfere with the experiment interpretation and measurements, WT PSEN1 and PSEN1 E280A ChLNs (obtained after 7 days in *Ch-N-Rm*) were left in a regular culture medium (RCm) for 4 additional days of post transdifferentiation (Mendivil-Perez et al. 2019).

Assay Protocol

An initial rotenone (ROT) screening was performed at least twice in triplicate including 1, 5, and 10 μ M final concentrations. Subsequently, 10 μ M ROT was established as an optimal concentration for further experiments. For analyses, ChLNs were divided into two groups: (i) untreated WT PSEN1; and (ii) WT PSEN1 treated with 10 μ M ROT. Chemical inhibition assay was performed by pre-incubating WT PSEN1 in absence or presence of cannabidiol (CBD; 10 μ M, Mendivil-Perez et al. 2023), the anthrapyrazolone JNK inhibitor SP600125 (SP; 1 μ M, Soto-Mercado et al. 2020), cell-permeable chemical inhibitor of p53 pifithrin- α

(PFT- α ; 50 nM, Velez-Pardo et al. 2002), and the potent and selective LRRK2 inhibitor PF-06447475 (PF475; 1 μ M, Mendivil-Perez et al. 2016) for 30 min previous to ROT exposure. The PSEN1 E280A ChLNs were used for comparative and validation purposes.

Immunofluorescence Analysis

The analysis of Alzheimer's disease-, oxidative stress- and cell death-related markers, was exactly performed as described elsewhere (Soto-Mercado et al. 2020). Briefly, the cells treated under different conditions were fixed with 4% paraformaldehyde for 20 min, followed by Triton X-100 (0.1%) permeabilization and 10% bovine serum albumin (BSA) blockage. Cells were incubated overnight with primary antibodies against the first 2 amino acids of the A β peptide amino N-terminus, namely the A β 4 1E8 antibody (1:500; clone 1E8 cat# MABN639, Millipore, 3050 Spruce Street, St. Louis, MO 63304, USA), phospho-TAU (p-Tau, 1:500, Ser²⁰²/Thr²⁰⁵, cat# MN1020 (AT8); and primary antibodies against oxidized DJ-1 (1:500; ox(Cys¹⁰⁶)DJ-1; spanning residue C¹⁰⁶ of human PARK7/DJ1; oxidized to produce cysteine sulfonic (SO₃) acid; cat # ab169520, Abcam). To assess cell death, we used primary antibodies against PUMA conjugated with Alexa Fluor 488 (1:500; PUMA, sc-377015 AF488, Santa Cruz Biotechnology), p53 conjugated with Alexa Fluor 594 (1:500; cat# sc-126 AF594, Santa Cruz Biotechnology), phospho-c-Jun conjugated with Alexa fluor 594 (1:500; c-Jun (S⁶³/T⁷³) cat# sc-822 AF594, Santa Cruz Biotechnology), and caspase-3 fluorescent probe (1:500; AM- DEV-FMK- caspase 3, V35118). To evaluate α -synuclein, we used primary antibodies against total α -synuclein (1:500; clone Syn211 cat# S5566, Sigma Aldrich), and phosphorylated α -synuclein (1:500; phosphoS¹²⁹; cat# ab51253, Abcam). After exhaustive rinsing, we incubated the cells with secondary fluorescent antibodies (to identify non-conjugated antibodies reactions; DyLight 488 and 594 horse anti-rabbit, -goat and -mouse, cat DI 1094, DI 3088, and DI 2488, respectively) at 1:500. The nuclei were stained with 1 μ M Hoechst 33,342 (Life Technologies), and images were acquired on an Axiovert coupled to AxioCam microscope.

Flow Cytometry Analysis

After each treatment, cells were detached using trypsin and centrifuged for 10 min at 2000 rpm. Then, cells were washed with PBS and fixed with cold ethanol (96%) overnight. Cells were washed two times with PBS and permeabilized with 0.2% Triton X-100 plus 1.5% bovine serum albumin (BSA) for 30 min. Cells were incubated overnight with primary antibodies against the first 2 amino acids of the A β peptide amino N-terminus, namely the A β 4 1E8 antibody (1:500;

clone 1E8 cat# MABN639, Millipore, 3050 Spruce Street, St. Louis, MO 63304, USA), phospho-TAU (AT8; 1:200), oxidized DJ-1 (1:200), PUMA (1:200), p53 (1:200), phospho-c-Jun (1:200; c-Jun (S^{63/73}), caspase-3 (1:200), total α -synuclein (1:200) and phosphorylated α -synuclein (1:200). After exhaustive rinsing, we incubated the cells with secondary fluorescent antibodies (DyLight 488 and 594 horse anti-rabbit, -goat and -mouse, cat DI 1094, DI 3088, and DI 2488, respectively) at 1:500. Fluorescence analysis was performed on a BD LSRFortessa II flow cytometer (BD Biosciences). Cells without primary antibodies served as a negative control. For assessment, 10,000 events and quantitative data and figures were obtained using FlowJo 7.6.2 Data Analysis Software (TIBCO® Data Science). Events analysis was performed by determining the cell population (Forward Scatter analysis, Y axis) that exceeded the basal fluorescence (488 nm or 594 nm, X axis) of the negative control. Accordingly, density plots or histograms were created from event analysis.

Evaluation of Intracellular Reactive Oxygen Species (e.g., Hydrogen Peroxide, H₂O₂) by Fluorescence Microscopy

To assess the levels of intracellular ROS (H₂O₂), we used 2',7'-dichlorofluorescein diacetate (5 μ M, DCFH₂-DA; Invitrogen) according to Soto-Mercado et al. 2020. ChLNs were left in RCm for 4 days. Then, the cells (5 \times 10³) were incubated with the DCFH₂-DA reagent for 30 min at 37 °C in the dark. Cells were then washed, and DCF fluorescence intensity was determined by analysis of fluorescence microscopy images (Lichtman and Conchello 2005). The assessment was repeated three times in independent experiments. The nuclei were stained with 0.5 μ M Hoechst 33,342 staining compound. The assessment was repeated three times in independent experiments blind to the experimenter.

Evaluation of Intracellular Hydrogen Peroxide (H₂O₂) by Flow Cytometry

To assess the levels of intracellular ROS (H₂O₂), we used 2',7'-dichlorofluorescein diacetate (5 μ M, DCFH₂-DA; Invitrogen) according to Soto-Mercado et al. 2020. ChLNs were left in RCm for 4 days. Then, the cells (1 \times 10⁴) were incubated with the DCFH₂-DA reagent for 30 min at 37 °C in the dark. Cells were then washed, and DCF fluorescence was determined using an LSRFortessa (BD Biosciences). The assessment was repeated 3 times in independent experiments. Quantitative data and figures were obtained using FlowJo 7.6.2 Data Analysis Software. The assessment was repeated three times in independent experiments blind to experimenter and flow cytometer analyst (Adan et al. 2017).

Analysis of Mitochondrial Membrane Potential ($\Delta\Psi$ m) by Fluorescence Microscopy

ChLNs were left in a regular culture medium (RCm) for 4 days. Then, the cells (5 \times 10³) were incubated with the passively diffusing and active mitochondria-accumulating dye deep red MitoTracker compound (20 nM, final concentration) for 20 min at RT in the dark (cat # M22426, Invitrogen, Soto-Mercado et al. 2020). Cells were then washed twice with PBS. MitoTracker fluorescence intensity was determined by analysis of fluorescence microscopy images (Lichtman and Conchello 2005). The assessment was repeated three times in independent experiments. The nuclei were stained with 0.5 μ M Hoechst 33,342 staining compound. The assessment was repeated three times in independent experiments blind to the experimenter.

Analysis of Mitochondrial Membrane Potential ($\Delta\Psi$ m) by Flow Cytometry

ChLNs were left in a regular culture medium (RCm) for 4 days. Then, the cells (1 \times 10⁴) were incubated with the passively diffusing and active mitochondria-accumulating dye deep red MitoTracker compound (20 nM, final concentration) for 20 min at RT in the dark (cat # M22426, Invitrogen, (Soto-Mercado et al. 2020). The cells were analyzed using an LSRFortessa (BD Biosciences). The experiment was performed three times in independent experiments, and 10,000 events were acquired for analysis. Quantitative data and figures were obtained using FlowJo 7.6.2 Data Analysis Software. The assessment was repeated three times in independent experiments blind to experimenter and flow cytometer analyst.

Intracellular Calcium Imaging

Intracellular calcium (Ca²⁺) concentration changes evoked by cholinergic stimulation were assessed according to Sekiguchi-Tonosaki et al. 2009 and Pap et al. 2009, with minor modifications. For the measurement, the fluorescent dye Fluo-3 (Fluo-3 AM; Thermo Fisher Scientific, cat: F1242) was employed. The dye was dissolved in DMSO (1 mM) to form a stock solution. Before the experiments, the stock solution was diluted in neuronal buffer solution (NBS buffer in mM: 137 NaCl, 5 KCl, 2.5 CaCl₂, 1 MgCl₂, pH 7.3, and 22 glucose). The working concentration of the dye was 2 μ M. The WT and PSEN1 E280A ChLNs were incubated for 30 min at 37 °C with the dye containing NBS and then washed five times. Intracellular Ca²⁺ transients were evoked by acetylcholine (1 mM final concentration) at 4 days post differentiation. The measurements were carried out using the 20 \times objective of the microscope. Several regions of interest (ROIs) were defined in the visual field of the camera. One

of the ROIs was cell free, and the fluorescence intensity measured here was considered background fluorescence ($F_{\text{background}}$). The time dependence of the fluorescence emission was acquired, and the fluorescence intensities (hence the Ca^{2+} levels) were represented by pseudo colors. To calculate the changes of the average Ca^{2+} -related fluorescence intensities, the F_{bg} value was determined from the cell-free ROI, and then the resting fluorescence intensities (F_{rest}) of the cell-containing ROIs were obtained as the average of the points recorded during a consecutive period of 10 s before the addition of acetylcholine. The peaks of the fluorescence transients were found by calculating the average of six consecutive points and identifying those points that gave the highest average value (F_{max}). The amplitudes of the Ca^{2+} -related fluorescence transients were expressed relative to the resting fluorescence ($\Delta F/F$) and were calculated by the following formula: $\Delta F/F = (F_{\text{max}} - F_{\text{rest}}) / (F_{\text{rest}} - F_{\text{bg}})$. For the calculation of the fluorescence intensities, ImageJ was used. The terms fluorescence intensity was used as an indirect indicator of intracellular Ca^{2+} concentration. The assessment was repeated three times in independent experiments blind to the experimenter.

Photomicrography and Image Analysis

Light microscopy photographs were taken using a Zeiss Axio Vert.A1 coupled to AxioCam Cm1 microscope, and fluorescence microscopy photographs were taken using a Zeiss Axio Vert.A1 Fluorescence Microscope equipped with a Zeiss AxioCam Cm1. Fluorescence images were transformed into 8-bit images and the background was subtracted (Zen 3.4 blue edition). Images were then analyzed by ImageJ software (<http://imagej.nih.gov/ij/>) using an in house-made macro. Briefly, the cellular measurement regions of interest (ROIs) were drawn around the nucleus (for the case of transcription factors and apoptosis effectors) or overall cells (for cytoplasmic probes), and the fluorescence intensity was subsequently determined by applying the same threshold for cells in the control and treatment conditions. Mean fluorescence intensity (MFI) was obtained by normalizing total fluorescence to the number of nuclei.

Molecular Docking

We used the x-ray diffraction crystallography protein structure of γ -secretase (protein data bank, PDB, code: 5FN2, (Bai et al. 2015) for molecular docking analysis. The blind molecular docking was performed with CB-Dock version 2 (Liu et al. 2022), a cavity detection-guided protein–ligand blind docking web server that uses Autodock Vina (version 1.1.2, Scripps Research Institute, La Jolla, USA). The Standard Delay Format (SDF) of the chemical structure of the tested compounds (rotenone, SCH 697466, MRK560, SCH 900229, LY-374973) were

downloaded from PubChem. The molecular blind docking was performed by uploading the 3D structure PDB file of listed protein into the server with the SDF file of each compound. For analysis, we selected the docking poses with the strongest Vina score in the catalytic pocket. The generated PDB files of the molecular docking of each compound were visualized with the CB-Dock2 interphase and were compared against the experimentally validated X-ray structures of the interaction with reference compounds.

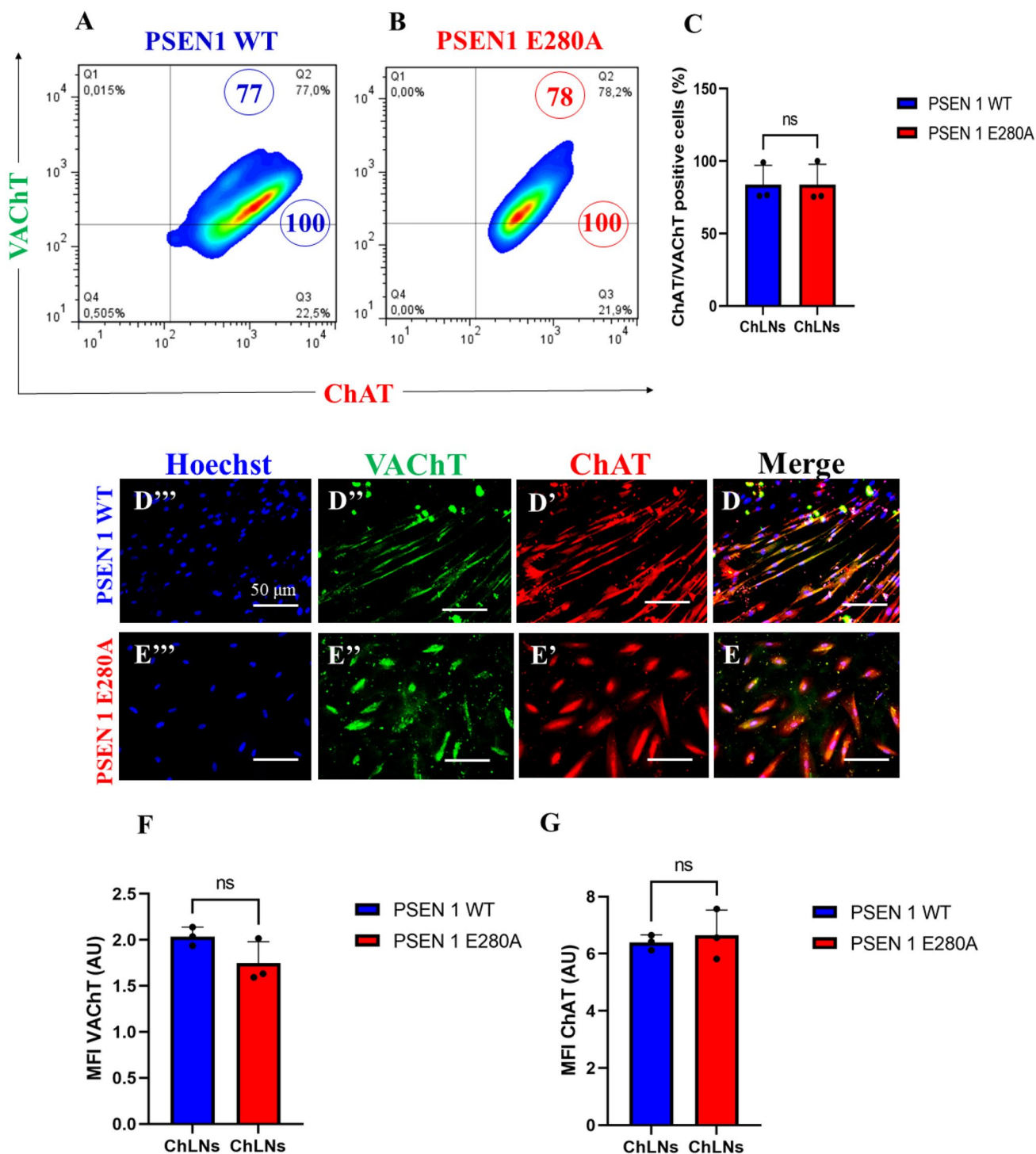
Data Analysis

In this experimental design, two vials of MSCs were thawed (WT PSEN1 and PSEN1 E280A), cultured and the cell suspension was pipetted at a standardized cellular density of 2.6×10^4 cells/cm² into different wells of a 24-well plate. Cells (i.e., the biological and observational unit (Lazic et al. 2018) were randomized to wells by simple randomization (sampling without replacement method), and then wells (i.e., the experimental units) were randomized to treatments by a similar method. Experiments were performed on three independent occasions (n=3) blind to the experimenter and/or flow cytometer analyst (Lazic et al. 2018). The data from the three repetitions i.e., independent experiments were averaged and a representative flow cytometry density or histogram plot from the three independent experiments was selected for illustrative purposes, whereas bar in quantification figures represent the mean \pm SD and the three black dots show data point of each experimental repetition. Based on the assumption that the experimental unit (i.e., the well) data comply with the independence of observations, the dependent variable is normally distributed in each treatment group (Shapiro–Wilk test), and variances are homogeneous (Levene’s test), the statistical significance was determined by one-way analysis of variance (ANOVA) followed by Tukey’s post hoc comparison calculated with GraphPad Prism 5.0 software. Differences between groups were only deemed significant when a p-value of <0.05 (*), <0.001 (**), and <0.001 (***). All data are illustrated as the mean \pm S.D.

Results

Wild Type (WT) and PSEN 1 E280 Warthon Jelly’s Mesenchymal Stromal Cells (WJ MSCs)-Derived Cholinergic-Like Cells (ChLNs) Show Typical Markers of Cholinergic Lineage

We first wanted to confirm that the mutation PSEN 1 E280A did not alter the transdifferentiation of WJ-MSCs into ChLNs cultured in *Ch-N-Run* medium (Soto-Mercado et al. 2020; Mendivil-Perez et al. 2023). Effectively, WT and mutant WJ-MSCs transdifferentiated into ChLNs in *Cholinergic-N-Run* yielding 75% cholinergic markers



ChAT/ VChT according to flow cytometry analysis (Fig. 1A-C). The cholinergic lineage markers were also detected by fluorescent microscopy (Fig. 1D-G). For comparative and validation purposes, we included the PSEN1 E280A ChLNs (Soto-Mercado et al. 2020; Mendivil-Perez et al. 2023).

Rotenone (ROT) Provokes Loss of Mitochondrial Membrane Potential ($\Delta\Psi_m$) and Generation of Reactive Oxygen Species (ROS)

It is well-known that ROT induces ROS/H₂O₂ through inhibition of mitochondrial Complex I (Li et al. 2003; Read

Fig. 1 Wild type (WT) and PSEN 1 E280A Warthon Jelly's Mesenchymal Stromal Cells (WJ MSCs)-derived Cholinergic-Like cells (ChLNs) show typical markers of cholinergic lineage. WT PSEN1 and PSEN1 E280A MenSCs Warthon Jelly's Mesenchymal Stromal Cells (WJ MSCs) were cultured in a cholinergic differentiation medium as described in the *Materials and Methods* section for 7 days. Cells were double stained with primary antibodies against the cholinergic lineage proteins vacuole acetylcholine transporter (VAcHT) and cholinergic acetylcholine transferase (ChAT). Representative flow cytometry density plots showing **A** VAcHT+/ChAT+PSEN1 WT ChLNs, **B** VAcHT+/ChAT+PSEN1 E280A ChLNs. **C** Percentage of VAcHT- and ChAT-positive cells in WT PSEN1 and PSEN1 E280A ChLNs. Representative fluorescence microscopy photographs showing **D** merge image of **D'** ChAT, **D''** VAcHT, and **D'''** Hoechst WT PSEN1 ChLNs; **E** merge image of **E'** ChAT, **E''** VAcHT, and **E'''** Hoechst PSEN1 E280A ChLNs. Positive blue fluorescence reflects nuclei, positive red fluorescence reflects the presence of ChAT, positive green fluorescence reflects the presence of VAcHT protein. **F** Mean fluorescence intensity (MFI) of VAcHT. **G** Mean fluorescence intensity (MFI) of ChAT. The data are presented as the mean \pm SD of three independent experiments ($n=3$). The figures represent 1 out of 3 independent experiments. One-way ANOVA followed by Tukey's test; n.s.=no statistically significance. Image magnification, 200 \times

et al. 2021). Therefore, we determined the concentration of ROT at which generates the maximal percentage of ROS and mitochondrial damage in ChLNs. As shown in Fig. 2, ROT induces concentration-dependent loss of $\Delta\Psi_m$ (Fig. 2A, B) and generation of ROS up to 5 μ M (Fig. 2C, D). Similar data were observed by fluorescent microscopy (Fig. 2E–N). Therefore, we selected ROT (10 μ M) for further experiments.

Rotenone (ROT) Induces Phosphorylation of Leucine-Rich Repeated Kinase 2 (LRRK2) Concomitantly with Phosphorylation of α -Synuclein at Pathological Residue Ser¹²⁹ in ChLNs

Next, we determined whether ROT induces p-LRRK2 concomitantly with p- α -Syn in ChLNs. To achieve this, ChLNs were exposed to ROT (10 μ M) for 24 h and then p-LRRK2 at residue Ser⁹³⁵ and p- α -Syn at residue Ser¹²⁹ were evaluated. Flow cytometry analysis reveals that ROT increased the phosphorylation of both LRRK2 by +363% (Fig. 3A, B) and α -Syn by +567% (Fig. 3C, D) compared to untreated ChLNs. Surprisingly, mutant ChLNs showed an important increased in p-LRRK2 (+225%), and p- α -Syn (+317%) compared to untreated ChLNs (Fig. 3A–D). Similar data were obtained by fluorescent microscopy analysis (Fig. 3E–L).

Rotenone (ROT) Induces Accumulation of iA β , Oxidized DJ-1 (DJ-1Cys¹⁰⁶-SO₃) and Phosphorylation of TAU at Pathological Residue Ser²⁰²/Thr²⁰⁵ in ChLNs

To characterize the neuronal expression of A β peptides in ChLNs under ROT exposure, we chose an antibody that has

previously been shown to be specific against A β ₄₂, namely the A β 4 1E8 antibody (Wiltfang et al. 2001; Maler et al. 2007). Thus, ChLNs were exposed to ROT (10 μ M) for 24 h and stained with the anti-amyloid A β 4 1E8. Figure 4 shows that ROT increased the accumulation of iA β by +386% (Fig. 4A, B), oxidized DJ-1 by +714% (Fig. 4C, D), and p-TAU at residue Ser²⁰²/Thr²⁰⁵ by +383% (Fig. 4E, F) compared to untreated ChLNs. As expected, mutant ChLNs increased accumulated iA β by +371%, DJ-1Cys¹⁰⁶-SO₃ by +814%, and p-TAU by +250% (Fig. 4A–F). Similar data was obtained by fluorescent microscopy (Fig. 4G–R).

Rotenone (ROT) Increases the Phosphorylation of c-JUN at Residues Ser⁶³/Ser⁷³ and the Expression of TP53, PUMA and CC3 in ChLNs

We determined whether ROT induces apoptotic markers p-JUN, TP53, PUMA, and CC3 in ChLNs (Mendivil-Perez et al. 2016). As shown in Fig. 6, ROT induced an important increase in the phosphorylation of p-JUN, expression TP53, PUMA, and CC3 by +311% (Fig. 5A, B), +457% (Fig. 5C, D), +600% (Fig. 5E, F), and +533% (Fig. 5G, H), respectively, in ChLNs. Compared to untreated WT, PSEN1 E280A also endogenously expressed p-JUN, TP53, PUMA, and CC3 by +167%, +314%, +412%, and +433%, respectively (Fig. 5A–H). Similar data were obtained by fluorescent microscopy (Fig. 5I–X).

Cannabidiol (CBD), SP600125 (SP), Pifithrin- α (PFT) and PF-06447475 (PF475) Block ROT-Induced Accumulation of iA β , Oxidized DJ-1, p-TAU Ser²⁰²/Thr²⁰⁵, p- α -Syn¹²⁹, and CC3, Respectively, in ChLNs

The above observations compelled us to evaluate whether the use of antioxidant or inhibitor compounds of critical molecules (e.g., iA β , DJ-1, TAU, α -Syn, CC3) diminish or augment ROT-induced signaling. To achieve this, ChLNs exposed to ROT alone or in combination with anti-amyloidogenic and antioxidant cannabidiol (CBD, 10 μ M), JNK inhibitor SP600125 (SP, 1 μ M), TP53 inhibitor pifithrin- α (PFT- α , 50 nM), and LRRK2 inhibitor PF-06447475 (PF475, 1 μ M) were evaluated for their effect on the accumulated iA β , oxDJ-1, p- α -Syn, p-TAU, and CC3, respectively. Figure 6 shows that CBD reduced the accumulation of iA β by -74% (Fig. 6A, B) and DJ-1Cys¹⁰⁶-SO₃ by -54% (Fig. 6C, D); SP diminished p-TAU at Ser²⁰²/Thr²⁰⁵ by -62% (Fig. 6E, F), PF475 abridged p- α -Syn at Ser¹²⁹ by -52% (Fig. 6G, H), and blunted CC3 by -82% (Fig. 6I, J). Last, PFT- α blocked CC3 by -54% (Fig. 6K, L). In addition, we assessed theoretically whether ROT binds to PSEN 1/ γ -secretase. For comparative purposes, we used well-known pharmacological inhibitors of PSEN 1/ γ -secretase complex e.g., SCH 697466, MRK560, SCH 900229, and GSI LY-374973 (Lee

Fig. 2 Rotenone (ROT) provokes loss of mitochondrial membrane potential ($\Delta\Psi_m$) and generation of reactive oxygen species (ROS). After 7 days of transdifferentiation, WT PSEN1 ChLNs were left untreated or treated with increasing concentrations of ROT (0, 1, 5, 10 μM) in regular culture medium (RCm) for 24 h. **A** Representative flow cytometry histogram showing DCF-positive (DCF+). **B** Quantification of DCF-positive cells by flow cytometry. **C** Representative flow cytometry histogram showing $\Delta\Psi_m$. **D** Quantification of $\Delta\Psi_m$ by flow cytometry. **E–H** Representative fluorescent microscopy showing WT PSEN1 ChLNs treated with ROT stained with MitoTracker™ Red. **I–L** Representative fluorescent microscopy showing WT PSEN1 ChLNs treated with ROT stained with DCF. Positive blue fluorescence reflects nuclei, positive red fluorescence reflects $\Delta\Psi_m$, positive green fluorescence reflects the presence of DCF+ cells. **M** Mean fluorescence intensity (MFI) of DCF-positive cells. **N** Mean fluorescence intensity (MFI) of $\Delta\Psi_m$. Data are expressed as mean \pm SD; Statistically significant differences when * $p < 0.05$; ** $p < 0.01$; *** $p < 0.001$. The figures represent 1 out of 3 independent experiments. Image magnification, 200 \times

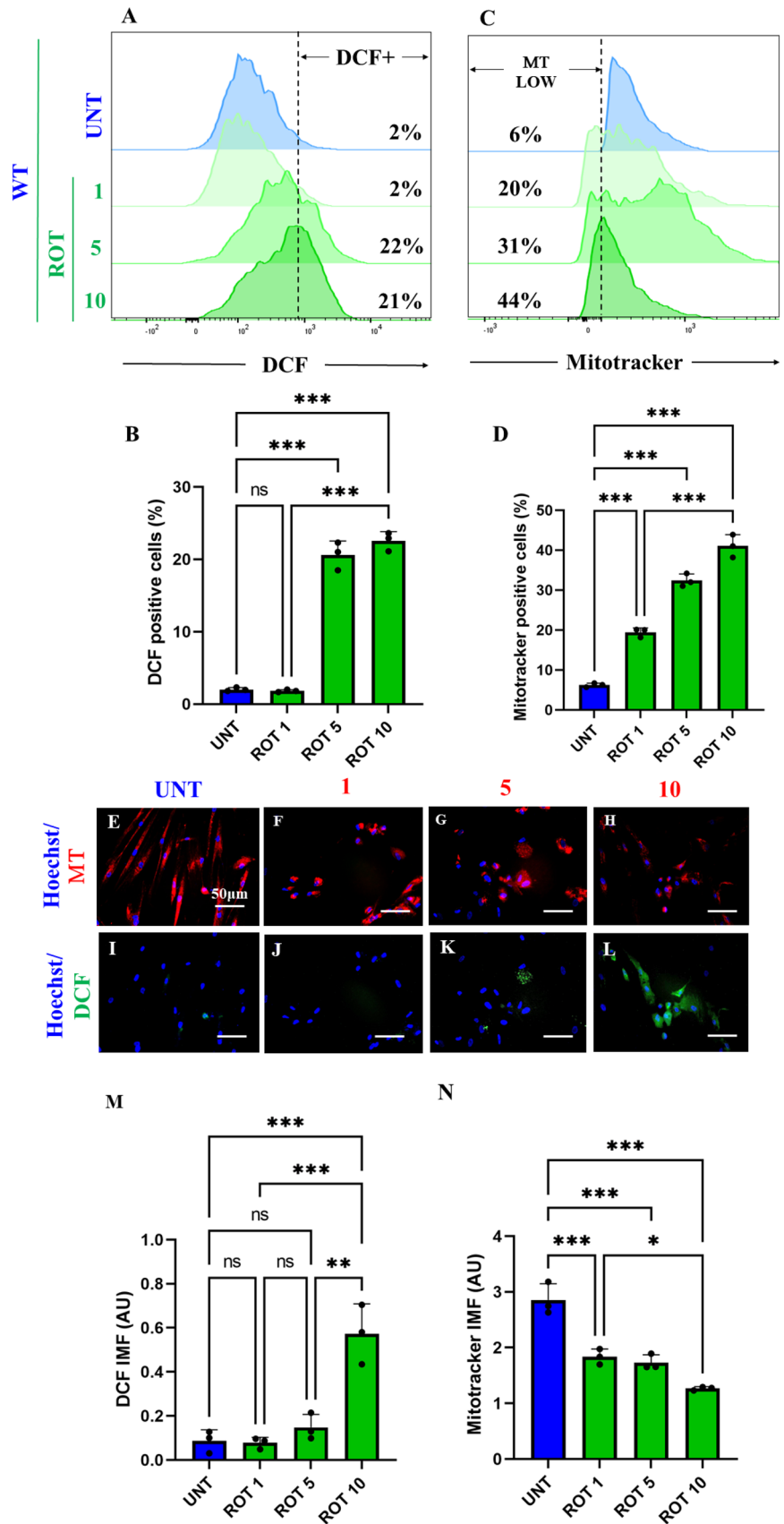


Fig. 3 Rotenone (ROT) induces phosphorylation of leucine-rich repeated kinase 2 (LRRK2) concomitantly with phosphorylation of α -synuclein at pathological residue Ser¹²⁹ in ChLNs. After 7 days of transdifferentiation, WT PSEN1 ChLNs were untreated or treated with ROT 10 μ M and PSEN1 E280A ChLNs were left in regular culture medium (RCm) for 24 h. **A** Representative flow cytometry histogram showing p-LRRK2. **B** Quantification of p-LRRK2-positive cells by flow cytometry. **C** Representative flow cytometry histogram showing p- α SYN. **D** Mean fluorescence intensity (MFI) of p- α SYN. **E–H** Representative fluorescence microscopy photographs showing **E** p-LRRK2 in untreated PSEN1 WT ChLNs or **F** treated with ROT. Representative fluorescence microscopy photographs showing **G** p-LRRK2-positive cells in PSEN1 E280A ChLNs. Positive blue fluorescence reflects nuclei, positive green fluorescence reflects the presence of p-LRRK2 protein. **H** Mean fluorescence intensity (MFI) of p-LRRK2. **I–K** Representative fluorescence microscopy photographs showing **I** p- α SYN in untreated PSEN1 WT ChLNs or **J** treated with ROT. Representative fluorescence microscopy photographs showing **K** p- α SYN -positive cells in PSEN1 E280A ChLNs. Positive blue fluorescence reflects nuclei, positive green fluorescence reflects the presence of p- α SYN protein. **L** Mean fluorescence intensity (MFI) of p- α SYN. Data are expressed as mean \pm SD; Statistically significant differences when * p < 0.05; ** p < 0.01; *** p < 0.001. The figures represent 1 out of 3 independent experiments. Image magnification, 200 \times

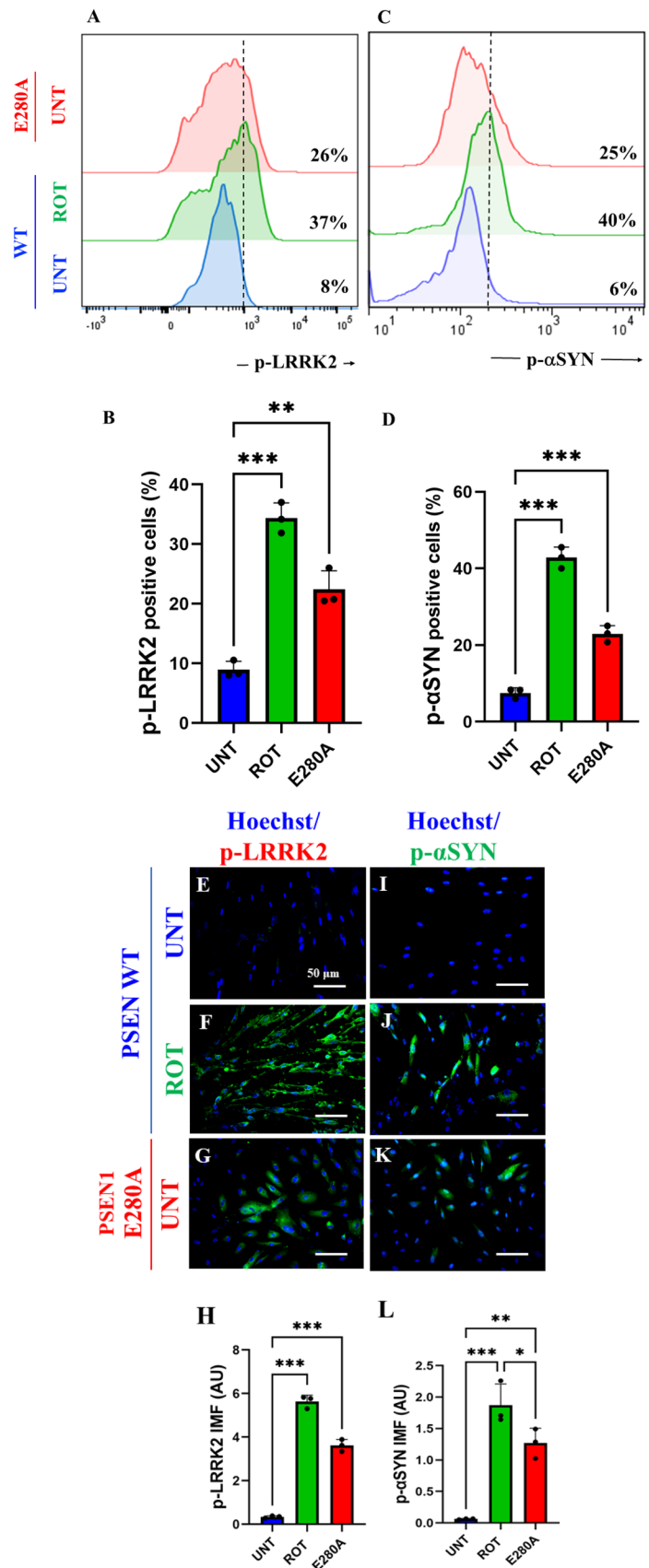
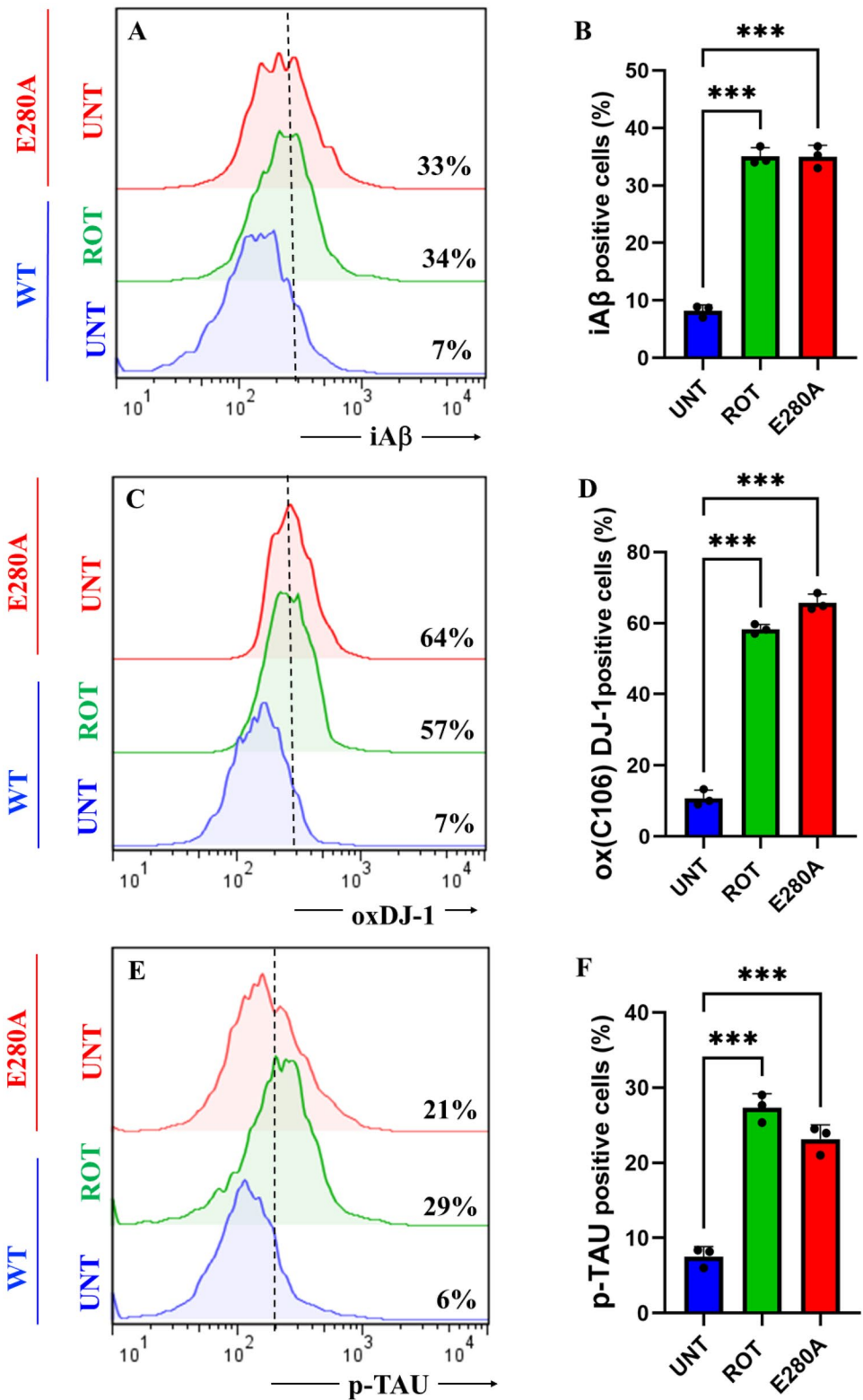


Fig. 4 Rotenone (ROT) induces accumulation of iA β , oxidized DJ-1 (DJ-1Cys¹⁰⁶-SO₃) and phosphorylation of TAU at pathological residue Ser²⁰²/Thr²⁰⁵ in ChLNs. After 7 days of transdifferentiation, WT PSEN1 ChLNs were untreated or treated with ROT 10 μ M and PSEN1 E280A ChLNs were left in regular culture medium (RCm) for 24 h. **A** Representative flow cytometry histogram showing iA β . **B** Quantification of iA β by flow cytometry. **C** Representative histogram showing oxDJ-1 by flow cytometry. **D** Mean fluorescence intensity (MFI) of oxDJ-1. **E** Representative histogram showing p-TAU by flow cytometry. **F** Mean fluorescence intensity (MFI) of p-TAU. **G–I** Representative fluorescence microscopy photographs showing **G** iA β in untreated PSEN1 WT ChLNs or **H** treated with ROT. Representative fluorescence microscopy photographs showing **I** iA β -positive cells in PSEN1 E280A ChLNs. Positive blue fluorescence reflects nuclei, positive red fluorescence reflects the presence of iA β protein. **J** Mean fluorescence intensity (MFI) of iA β . **K–M** Representative fluorescence microscopy photographs showing **K** Representative fluorescence microscopy photographs showing oxDJ-1 in untreated PSEN1 WT ChLNs or **L** treated with ROT. Representative fluorescence microscopy photographs showing **M** oxDJ-1-positive cells in PSEN1 E280A ChLNs. Positive blue fluorescence reflects nuclei, positive green fluorescence reflects the presence of oxDJ-1 protein. **N** Mean fluorescence intensity (MFI) of oxDJ-1. **O–R** Representative fluorescence microscopy photographs showing **O** p-TAU in untreated PSEN1 WT ChLNs or **P** treated with ROT. Representative fluorescence microscopy photographs showing **Q** p-TAU-positive cells in PSEN1 E280A ChLNs. Positive blue fluorescence reflects nuclei, positive red fluorescence reflects the presence of p-TAU protein. **R** Mean fluorescence intensity (MFI) of p-TAU. Data are expressed as mean \pm SD; Statistically significant differences when * p <0.05; ** p <0.01; *** p <0.001. The figures represent 1 out of 3 independent experiments. Image magnification, 200 \times



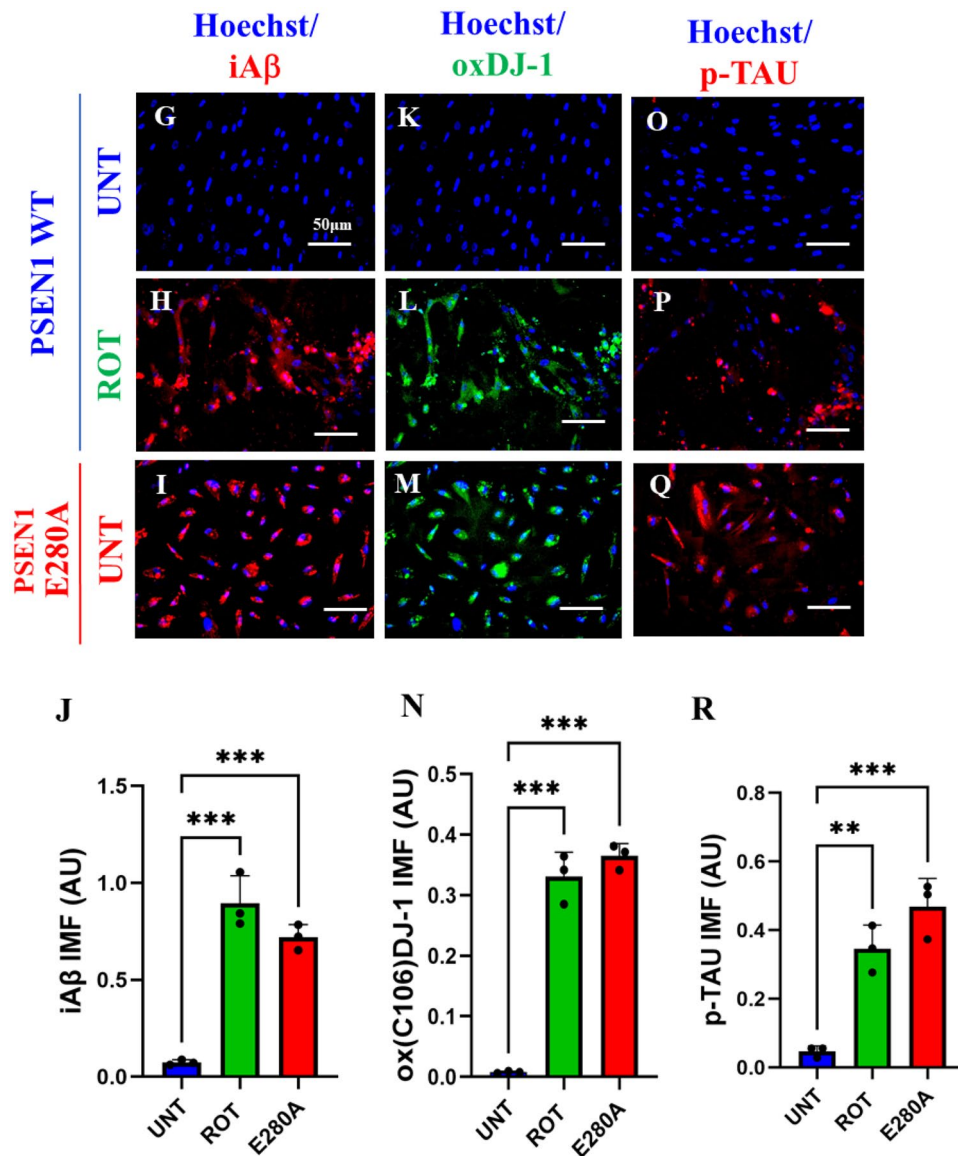


Fig. 4 (continued)

et al. 2011; Wu et al. 2012; Hyde et al. 2013; Sogorb-Esteve et al. 2018; Serneels et al. 2023). Molecular in silico docking analysis reveals that ROT (PubChem CID 6758) binds to catalytic pocket of PSEN1 (RSCB protein data bank e.g., 5FN2, (Bai et al. 2015)) with a binding affinity of -8.0 (kcal / mol) Vina score (Fig. 7A and Table 1) compare to the high binding affinity displayed by the γ -secretase inhibitor e.g., SCH 697466 (-9.2 Vina Score, Fig. 7B and Table 1; (Hyde et al. 2013). Interestingly, other binding affinities for PSEN1 inhibitors e.g., MRK560 (Lee et al. 2011), SCH 900229 (Wu et al. 2012), and GSI LY-374973 (Sogorb-Esteve et al. 2018) were near to the binding Vina Score of ROT (Table 1).

Rotenone (ROT) Impairs ACh-induced Transient Ca²⁺ Influx in ChLNs

We further evaluated whether ROT alters ChLNs response to ACh stimuli as an assessment of cholinergic neuronal Ca²⁺ responsiveness and functionality (Deutch and Roth 2014). To achieve this, ChLNs were left untreated or treated with ROT. Figure 8 shows that ACh stimulated a transient increase in intracellular Ca²⁺ in untreated ChLNs (Fig. 8A, $\Delta F/F = 23.5 \pm 0.3$, mean duration = 20 s; n = 20 ChLNs imaged, N = 3 dishes, Fig. 8D, E). In the presence of ROT, the Ca²⁺ influx was greatly reduced after ACh addition into ChLNs (Fig. 8B, D, $\Delta F/F = 6.00 \pm 0.8$,

Fig. 5 Rotenone (ROT) increases the phosphorylation of c-JUN at residues Ser⁶³/Ser⁷³ and the expression of TP53, PUMA and CC3 in ChLNs. After 7 days of trans-differentiation, WT PSEN1 ChLNs were untreated or treated with ROT 10 μM and PSEN1 E280A ChLNs were left in regular culture medium (RCm) for 24 h.

A Representative flow cytometry histogram showing p-JUN. **B** Mean fluorescence intensity (MFI) of p-JUN.

C Representative flow cytometry histogram showing TP53. **D** Mean fluorescence intensity (MFI) of TP53-positive cells.

E Representative flow cytometry histogram showing PUMA. **F** Mean fluorescence intensity (MFI) of PUMA-positive cells.

G Representative flow cytometry histogram showing CC3. **H** Mean fluorescence intensity (MFI) of CC3-positive cells.

I–K Representative fluorescence microscopy photographs showing **I** p-JUN in untreated PSEN1 WT ChLNs or **J** treated with ROT. Representative fluorescence microscopy photographs showing **K** p-JUN-positive cells in PSEN1 E280A ChLNs. Positive blue fluorescence reflects nuclei, positive red fluorescence reflects the presence of p-JUN protein.

L Mean fluorescence intensity (MFI) of p-JUN. **M–O** Representative fluorescence microscopy photographs showing

M PUMA in untreated PSEN1 WT ChLNs or **N** treated with ROT. Representative fluorescence microscopy photographs showing

O PUMA-positive cells in PSEN1 E280A ChLNs. Positive blue fluorescence reflects nuclei, positive green fluorescence reflects the presence of PUMA protein.

P Mean fluorescence intensity (MFI) of PUMA. **Q–T** Representative fluorescence microscopy photographs showing

Q TP53 in untreated PSEN1 WT ChLNs or **R** treated with ROT. Representative fluorescence microscopy photographs showing

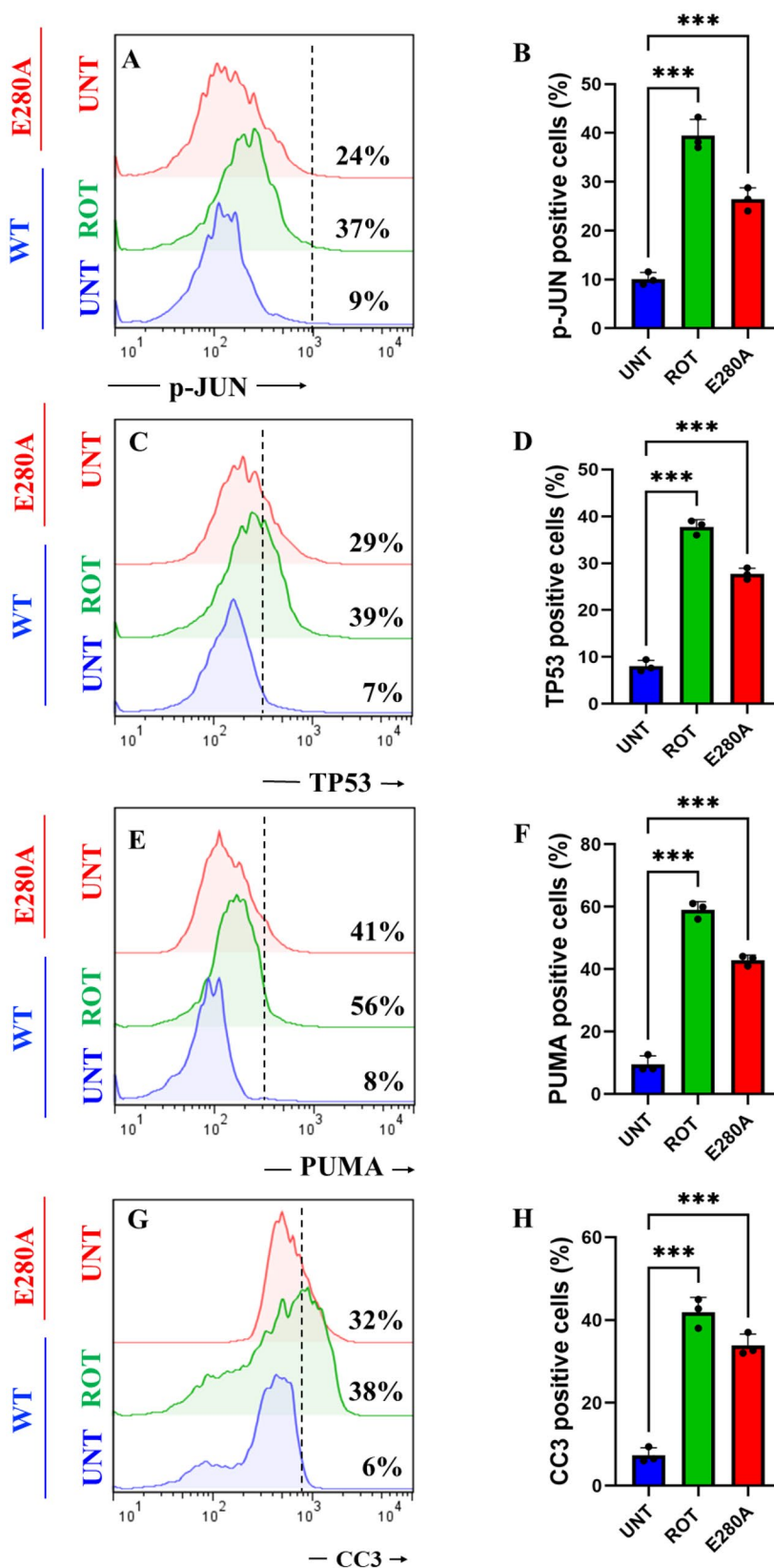
S TP53-positive cells in PSEN1 E280A ChLNs. Positive blue fluorescence reflects nuclei, positive red fluorescence reflects the presence of TP53 protein.

T Mean fluorescence intensity (MFI) of TP53. **U–W** Representative fluorescence microscopy photographs showing

U CC3 in untreated PSEN1 WT ChLNs or **V** treated with ROT. Representative fluorescence microscopy photographs showing

W CC3-positive cells in PSEN1 E280A ChLNs. Positive blue fluorescence reflects nuclei, positive green fluorescence reflects the presence of CC3 protein.

X Mean fluorescence intensity (MFI) of CC3. Data are expressed as mean ± SD; Statistically significant differences when *p < 0.05; ** p < 0.01; ***p < 0.001. The figures represent 1 out of 3 independent experiments. Image magnification, 200×



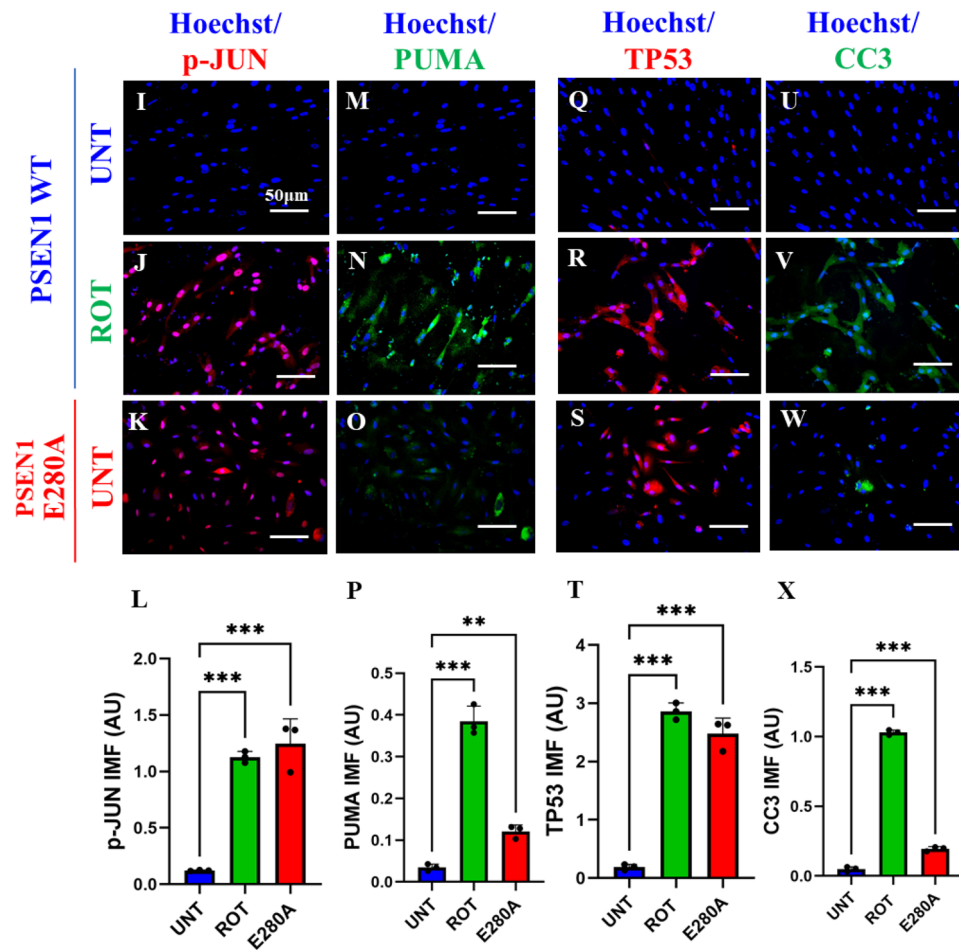


Fig. 5 (continued)

mean duration = 20 s; n = 20 ChLNs imaged, N = 3 dishes Fig. 8E). As expected, ACh did not affect intracellular dysfunctional Ca^{2+} influx in PSEN1 E280A ChLNs, used as control (Fig. 8C, $\Delta F/F = 0.50 \pm 0.02$, mean duration = 20 s; n = 20 ChLNs imaged, N = 3 dishes, Fig. 8D, E). We then theoretically inquired whether ROT might bind to $\alpha 7$ nicotinic cholinergic receptors ($\alpha 7\text{nChR}$), a cation permeable ligand-gated ion channels with a high permeability to Ca^{2+} (Noviello et al. 2021), which is implicated in AD (Singh et al. 2024). Molecular in silico docking analysis reveals that ROT binds to $\alpha 7\text{nChR}$ with high affinity (-7.6 Vina score, Table 1) compared to e.g., methyllycaconitine (-7.2 Vina score, Table 1), a selective and potent antagonist of the $\alpha 7\text{nAChR}$ at the α -bungarotoxin binding site (Ward et al. 1990).

Discussion

In this study, we provide evidence that ROT induced the expression of the typical neuropathological hallmarks α -Syn, TAU, and $i\text{A}\beta$ in vitro cell model ChLNs. Interestingly, those pathological markers were found in PDD humans' brains (Smith et al. 2019). Therefore, PDD is a neurological condition that recapitulates PD and AD (Goetz et al. 2009; Irwin et al. 2013; Jellinger 2023). Although previous studies have reported that ROT induces protein aggregation containing $\text{A}\beta$, p- α -Syn and hyperphosphorylated TAU in cultured cells of hippocampus, substantia nigra and locus coeruleus (Chaves et al. 2010, 2016), no further attempts were made to explain the mechanism by which ROT simultaneously triggers the coexistence of $i\text{A}\beta$, TAU, and

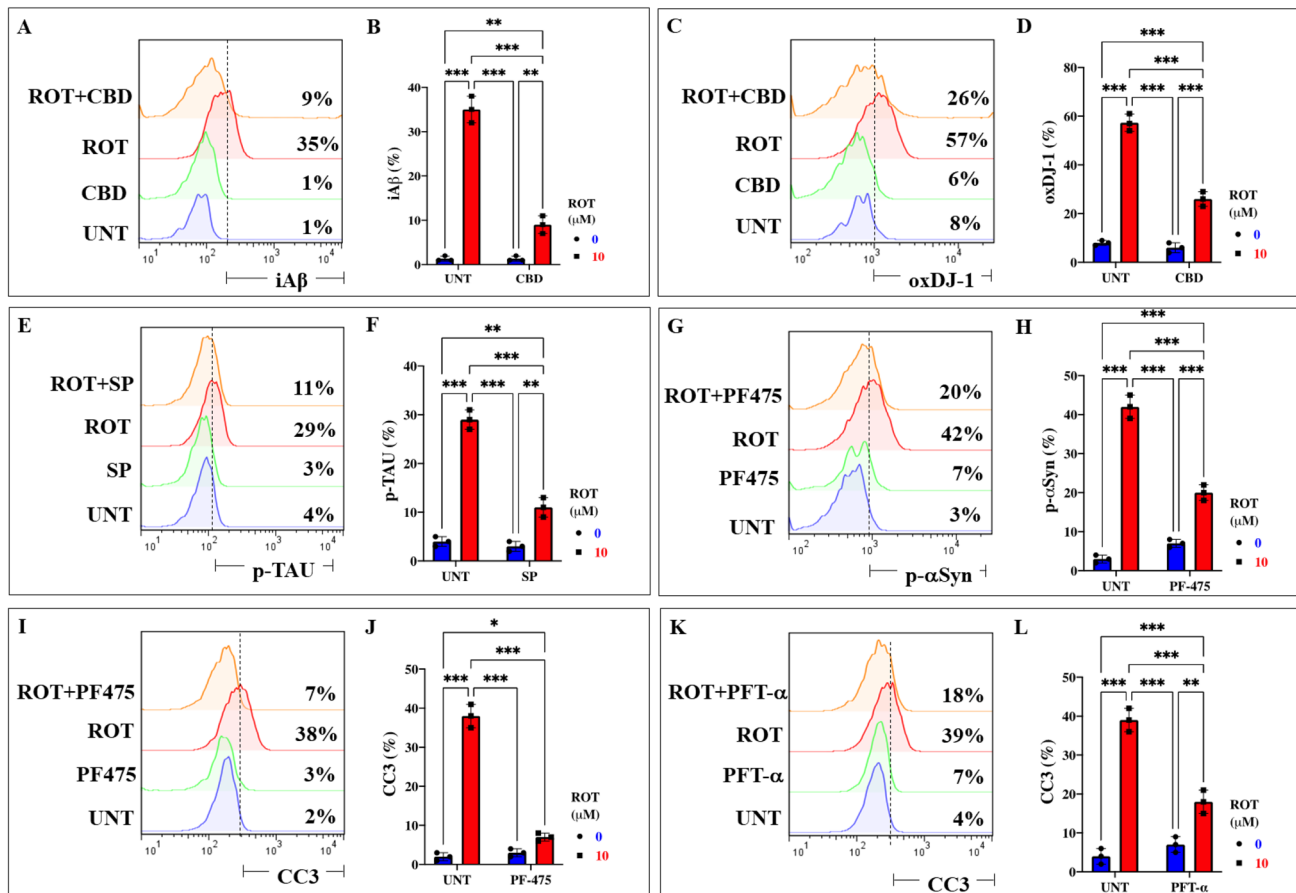


Fig. 6 Cannabidiol (CBD), SP600125 (SP), pifithrin- α (PFT), and PF-06447475 (PF475) block ROT-induced accumulation of iA β , oxidized DJ-1, p-TAU, p- α -Syn¹²⁹, and CC3, respectively, in ChLNs. After 7 days of transdifferentiation, WT PSEN1 ChLNs were untreated or treated with ROT, with CBD (10 μ M), SP (1 μ M), and PF475 (1 μ M) in regular culture medium (RCm) for 24 h. **A** Representative flow cytometry histogram showing iA β in untreated WT PSEN1 or treated untreated with ROT only, CBD only, or with ROT and CBD. **B** Percentage of iA β -positive cells by flow cytometry. **C** Representative flow cytometry histogram showing oxDJ-1 in untreated PSEN1 WT or treated with ROT only, CBD only, or with ROT and CBD. **D** Percentage of oxDJ-1-positive cells by flow cytometry. **E** Representative flow cytometry histogram showing p-TAU in

untreated PSEN1 WT or treated with ROT only, SP only, or with ROT and SP. **F** Percentage of p-TAU-positive cells by flow cytometry. **G** Representative flow cytometry histogram showing p- α -Syn in untreated PSEN1 WT or treated with ROT only, PF475 only, or with ROT and PF475. **H** Percentage of p- α -Syn -positive cells by flow cytometry. **I** Representative flow cytometry histogram showing CC3 in untreated PSEN1 WT or treated with ROT only, PF475 only, or with ROT and PF475. **J** Percentage of CC3-positive cells by flow cytometry. **K** Representative flow cytometry histogram showing CC3 in untreated PSEN1 WT or treated with ROT only, PFT- α only, or with ROT and PFT- α . **L** Percentage of p- α -Syn -positive cells by flow cytometry. Data are expressed as mean \pm SD; Statistically significant differences when * p < 0.05; ** p < 0.01; *** p < 0.001

α -Syn. Here, we show for the first time that ROT-induced coexistence of iA β , p-TAU^{202/Thr²⁰⁵}, p- α -Syn¹²⁹, and apoptosis signaling in ChLNs triggered by a cascade of molecular signaling, involving the oxidation of DJ-1 (DJ-Cys¹⁰⁶-SO₃), phosphorylation of LRRK2⁹³⁵, activation of transcription factors c-JUN and TP53, expression of BH-3-only protein PUMA, loss of $\Delta\Psi$ m, and activation of CASP3. Furthermore, we found that LRRK2 kinase, c-Jun N-terminal kinase (JNK) signaling, ROT itself, and TP53/c-JUN/PUMA are implicated in the phosphorylation of α -Syn, p-TAU, impairment of PSEN1/ γ -secretase complex), and apoptosis, respectively, in

ChLNs. These findings might be of importance for the understanding of the mechanism(s) of neuronal cell death not only in PDD, but also in PD (Dong-Chen et al. 2023) and AD (Golde 2009).

Mounting evidence have demonstrated that ROT generates ROS/ H₂O₂ (Li et al. 2003) through inhibition of mitochondrial complex I (Read et al. 2021). In turn, H₂O₂ operates via oxidation of susceptible Cys-SH residue on proteins, thereby, mediating intracellular redox-sensitive signal transduction (Marinho et al. 2014; Di Marzo et al. 2018). In fact, H₂O₂ -induced apoptotic cell death through direct or indirect activation of several pro-death signaling

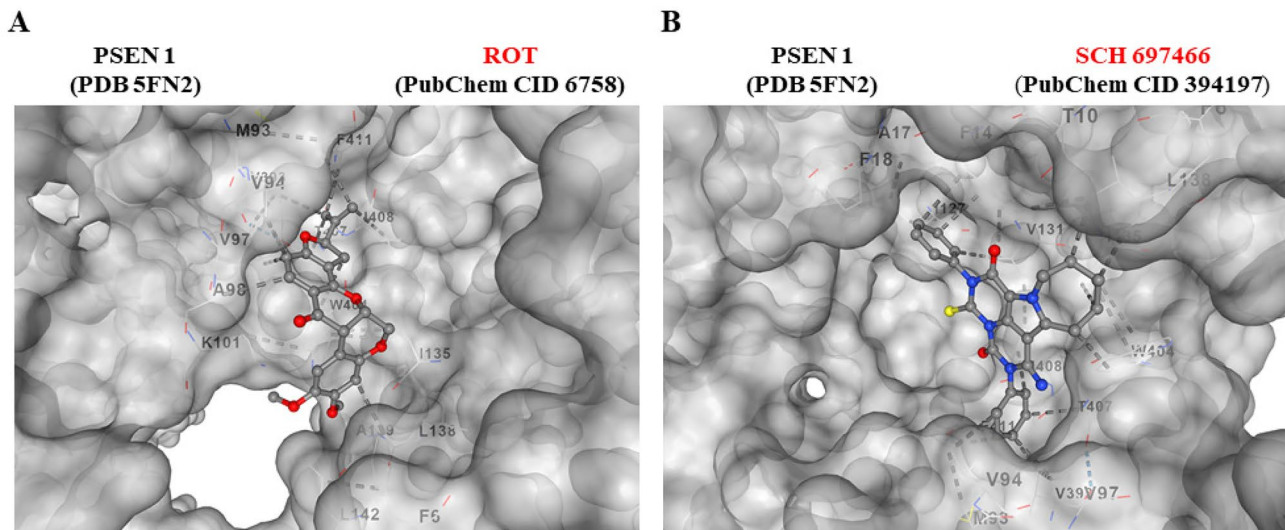


Fig. 7 Rotenone binds to PSEN1/ γ -secretase. **A** Representative CB-Dock2 3D images showing the molecular docking of PSEN1 (PDB: 5FN2) with rotenone compound. **B** Molecular docking of PSEN1 (PDB: 5FN2) with inhibitor SCH 697466 compound

molecules (Velez-Pardo and Jimenez-Del-Rio 2020), including kinases, transcription factors, and enzymes, among others. Here, we confirm that ROT induced concentration-dependent loss of $\Delta\Psi_m$, and generation of ROS/ H_2O_2 according to low-MitoTracker®-positive and DFC-positive ChLNs, respectively. Indeed, H_2O_2 not only induces depolarization of mitochondrial membrane (Takeyama et al. 2002) but also oxidizes the stress sensor protein DJ-1-Cys¹⁰⁶-SH (sulfhydryl group) into the DJ-1-Cys¹⁰⁶-SO₃ (sulfonic acid). Actually, the Cys¹⁰⁶-SH is the most sensitive cysteine residue in DJ-1 protein to H_2O_2 -mediated oxidation (Kinumi et al. 2004). We found that ROT significantly increase the oxidized DJ-1 in ChLNs. Given that DJ-1 plays an important role in PD (Repici and Giorgini 2019), oxidized DJ-1 has been postulate as a possible biomarker of PD (Saito 2017). However, whether oxidized DJ-1 might be an additional pathologic marker associated with PDD merits further investigation. Nonetheless, ROS/ H_2O_2 disable DJ-1 from its capacity to modulate signaling pathways related with neuroprotective actions (Neves et al. 2022). Indeed, the most accepted function for DJ-1 is a neuronal protective role against OS (Biosa et al. 2017). Interestingly, the antioxidant CBD (Hacke et al. 2019) significantly reduced the oxDJ-1 in ChLNs exposed to ROT. Moreover, CBD has been demonstrated to inhibit the activation of CASP3 (Mendivil-Perez et al. 2023). Taken together, these observations suggest that rising of ROS/ H_2O_2 play a critical role in the early stages of the pathophysiology of the PDD. Therefore, antioxidant therapy should not only be beneficial for PDD but also for PD (Andrade et al. 2023).

How does ROT link α -Syn, iA β , and Tau in ChLNs as model of PDD? Our findings suggest that ROT triggers three alternative and complementary mechanisms, involving the putative interaction between ROT and PSEN1/ γ -secretase, ROT-induced activation of JNK, and phosphorylation of LRRK2 kinase, which eventually converge on p- α -Syn, iA β , p-TAU, and apoptosis. Several observations support this. First, H_2O_2 might activate LRRK2 kinase activity by directly enhancing its autophosphorylation, e.g., at Tyr¹⁹⁶⁷ (Kamikawaji et al. 2009), Ser²⁰³², and Tyr²⁰³⁵ (West et al. 2007; Li et al. 2010), or indirectly, via phosphorylation of Ser⁹¹⁰ and Ser⁹³⁵ via the inhibitor of nuclear factor- κ B (I κ B) kinase (IKK) complex (Dzamko et al. 2012). In line with this, we found a significant increase p-Ser⁹³⁵ LRRK2 concomitant with an important increase of p-Ser¹²⁹ α -Syn in ChLNs exposed to ROT. These results suggest that, once active, the LRRK2 kinase phosphorylates α -Syn at Ser¹²⁹ (Qing et al. 2009), which is the major component of pathological deposits in PD (Fujiwara et al. 2002; Du et al. 2021). Of note, the inhibitor LRRK2 kinase PF-06447475 almost completely abolished the p-Ser¹²⁹- α -Syn. Taken together, these results suggest that p-Ser⁹³⁵ LRRK2 is implicated in the phosphorylation of α -Syn at residue Ser¹²⁹ in ChLNs treated with ROT (Qing et al. 2009). Second, H_2O_2 indirectly activates JNK kinase through activation of ASK-1 (Nadeau et al. 2009). In turn, JNK kinase phosphorylates TAU protein at Ser²⁰²/Thr²⁰⁵ (Reynolds et al. 2000), two amino acid residues implicated in TAU protein aggregation (Neddens et al. 2018). Interestingly, phosphorylation of TAU at residue Ser²⁰⁸, identified with antibody AT8 used in this

Table 1 In silico molecular docking analysis of ROT, inhibitor agents, and PSEN 1/ γ secretase

Submitted Protein ^a	Submitted Ligand ^b	Vina Score ^c	Cavity Volume (Å ³)	Center (x, y, z)	Docking size (x, y, z)	Contact residue
PSEN 1/ γ secretase (5FN2)	ROT (PubChem CID 6758)	-8.0	4571	128, 120, 115	35, 35, 35	Pocket C1 Chain B: MET93 VAL94 VAL97 ALA98 LYS101 VAL393 TRP404 THR407 ILE408 PHE411 Chain C: PHE6 ILE135 LEU138 ALA139 LEU142
PSEN 1/ γ secretase (5FN2)	SCH 697466 (PubChem CID 394197)	-9.2	4571	128, 120, 115	35, 35, 35	Pocket C1 Chain B: MET93 VAL94 VAL97 VAL393 TRP404 THR407 ILE408 PHE411 Chain C: PHE6 THR10 PHE14 ALA17 PHE18 ILE127 VAL131 ILE135 LEU138
PSEN 1/ γ secretase (5FN2)	MRK560 (PubChem CID 11577204)	-8.4	4571	128, 120, 115	35, 35, 35	Pocket C1 Chain B: THR90 MET93 VAL94 VAL97 VAL393 TRP404 THR407 ILE408 PHE411 VAL412 LEU415 Chain C: PHE14 ALA17 PHE18 PHE21 LEU35 VAL36 ILE127 ILE128 VAL131
PSEN 1/ γ secretase (5FN2)	SCH 900229 (PubChem CID 25164607)	-8.3	4571	128, 120, 115	35, 35, 35	Pocket C1 Chain B: VAL97 VAL393 TRP404 THR407 ILE408 PHE411 VAL412 LEU415 Chain C: PHE14 ALA17 PHE18 LEU35 VAL36 ALA39 ILE127 ILE128 VAL131 ILE135
PSEN 1/ γ secretase (5FN2)	LY-374973 (PubChem CID 5311272)	-8.3	4571	128, 120, 115	35, 35, 35	Pocket C1 Chain B: ILE143 MET146 THR147 LEU150 LEU166 SER169 SER170 LEU173 ILE229 MET233 ILE253 THR256 ASP257 ALA260 LYS265 LEU282 PHE283 LEU383 GLY384 ASP385 ILE387 PHE388
α 7nAChR (7KOQ)	ROT (PubChem CID 6758)	-7.6	6911	118, 140, 113	32, 34, 35	Pocket C2 Chain A: LYS45 ALA257 GLU258 MET260 ALA262 Chain B: ASP41 VAL42 GLU44 GLU172 TRP173 ARG205 TYR209 TYR210 LEU214 LEU255 VAL256 GLU258 ILE259
α 7nAChR (7KOQ)	Methyllycaconitine (PubChem CID 5288811)	-7.2	6911	118, 140, 113	32, 34, 35	Pocket C2 Chain A: LYS45 ASN46 ALA95 Chain B: MET40 ASP41 VAL42 ASP43 GLU44 LYS45 ASN46 VAL48 THR50 ILE122 LYS124 GLU258 ILE259

^aAccording to RCSB Protein Data Base (<https://www.rcsb.org/>)^bAccording to PubChem database (<https://pubchem.ncbi.nlm.nih.gov/>)^cAccording to CB-dock2: An accurate protein-ligand bind cocking tool (<https://cadd.labshare.cn/cb-dock2/php/index.php>)

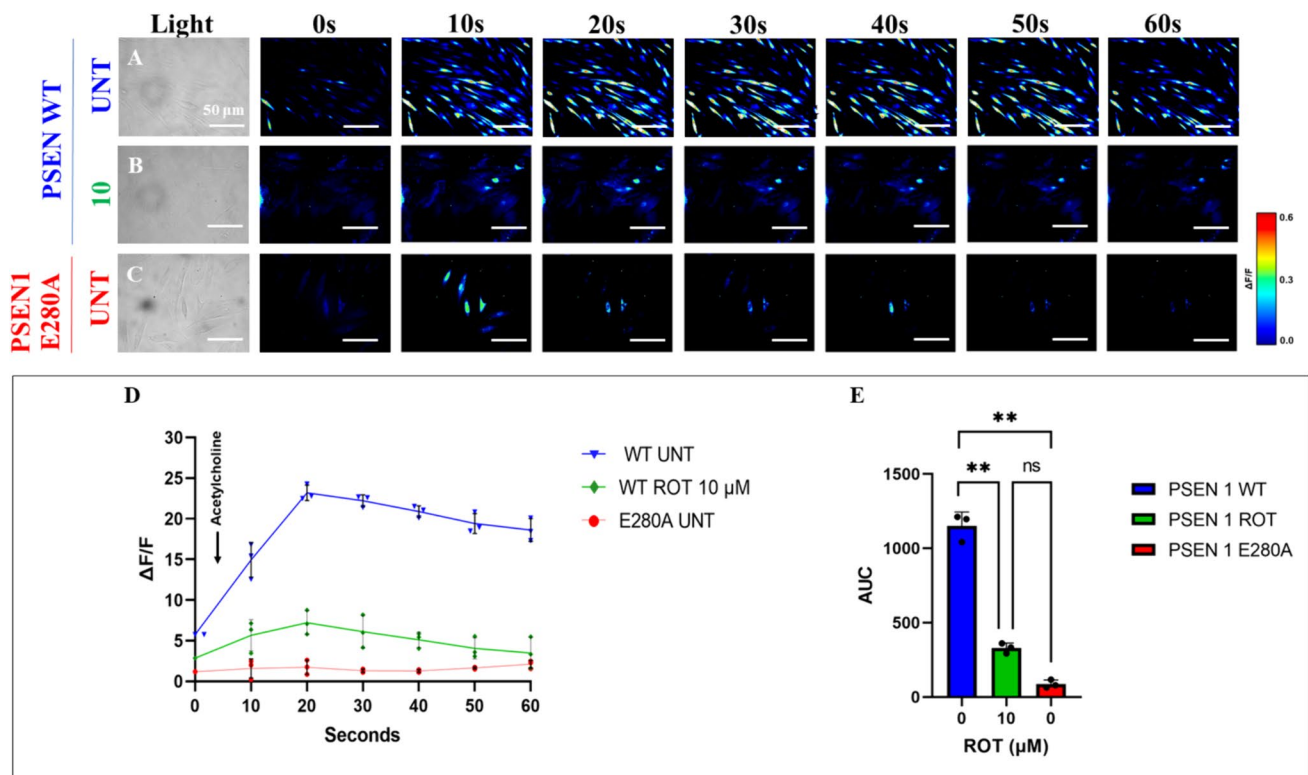


Fig. 8 Rotenone (ROT) impairs acetylcholine (ACh)-induced transient Ca^{2+} influx in ChLNs. After 7 days of transdifferentiation, WT PSEN1 ChLNs were untreated or treated with ROT 10 μM and PSEN1 E280A ChLNs were left in regular culture medium (RCM) for 24 h. **A–C** Time-lapse images (0, 10, 20, 30, 40, 50, and 60 s) of Ca^{2+} fluorescence in **A** untreated WT PSEN1 or **B** treated with ROT and **C** E280A ChLNs in response to ACh treatment. ACh was added to the culture at 0 s (arrow), and Ca^{2+} fluorescence of cells was moni-

tored at the indicated times. The color contrast indicates fluorescence intensity: dark blue < light blue < green < yellow < red. **D** Normalized mean fluorescence signal ($\Delta\text{F}/\text{F}$) over time from cells indicating temporally elevated cytoplasmic Ca^{2+} in response to ACh treatment; **E** Calculated area under the curve (AUC). Data are expressed as mean \pm SD; Statistically significant differences when ** $p < 0.01$. The figures represent 1 out of 3 independent experiments. Image magnification, 200 \times

work, also promotes aggregation and reveals neuropathologic diversity in Alzheimer's disease and other tauopathies (Xia et al. 2020). Indeed, the combined phosphorylation at the Ser²⁰²/Thr²⁰⁵/Ser²⁰⁸ sites produces a Tau sample that readily forms fibers (Despres et al. 2017). Inhibition of the JNK signaling pathway might avoid TAU hyperphosphorylation and aggregation. Accordingly, we found that JNK inhibitor SP600125 significantly reduced p-TAU in ChLNs treated with ROT. Therefore, JNK is a potential therapeutic target for PDD, PD and AD (Hepp Rehfeldt et al. 2020; Usmani et al. 2021; Zhu et al. 2022). Nonetheless, LRRK2 may also contribute to TAU hyperphosphorylation and aggregation (Shanley et al. 2015; Hamm et al. 2015). Third, ROT induces high levels of accumulated $\text{iA}\beta$ in ChLNs. However, the molecular mechanism by which ROT induces $\text{iA}\beta$ is not yet fully established. A possible explanation is that ROT binds to PSEN1/ γ -complex. Indeed, a molecular in silico docking analysis shows that ROT binds to a putative binding pocket in the PSEN1/ γ secretase with nearly similar binding Vina scores as those found with typical

reference synthetic inhibitor PSEN1/ γ secretase MRK560, SCH 900229, and LY-374973 (Table 1). Although not yet experimentally confirmed, it is predicted that ROT might be able to affect dynamic conformational changes that control progressive catalysis by PSEN1/ γ -secretase towards intracellular overproduction and accumulation of $\text{A}\beta$ (Svedružić et al. 2023). Indeed, the enzymatic activity of PSEN1/ γ -secretase is highly sensitive to structural changes induced by either PSEN1 mutations (Do et al. 2023) or γ secretase modulators GSM (Xia 2019). Interestingly, ROT displays mitochondrial off-target (e.g., binds to tubulin, Srivastava and Panda 2007) contributing to its toxic effects (Ren et al. 2005). Additionally, we found that CBD diminished accumulation of $\text{iA}\beta$ in ChLNs exposed to ROT. These observations suggest that CBD, in addition to operate as antioxidant, it also works as anti-amyloidogenic agent. Given that CBD possesses several pharmacological effects (Castillo-Arellano et al. 2023), this cannabinoid might be a potential therapeutic agent for the treatment of PDD (Ferreira-Junior et al. 2020; Zhang et al. 2022b; Mendivil-Perez et al. 2023).

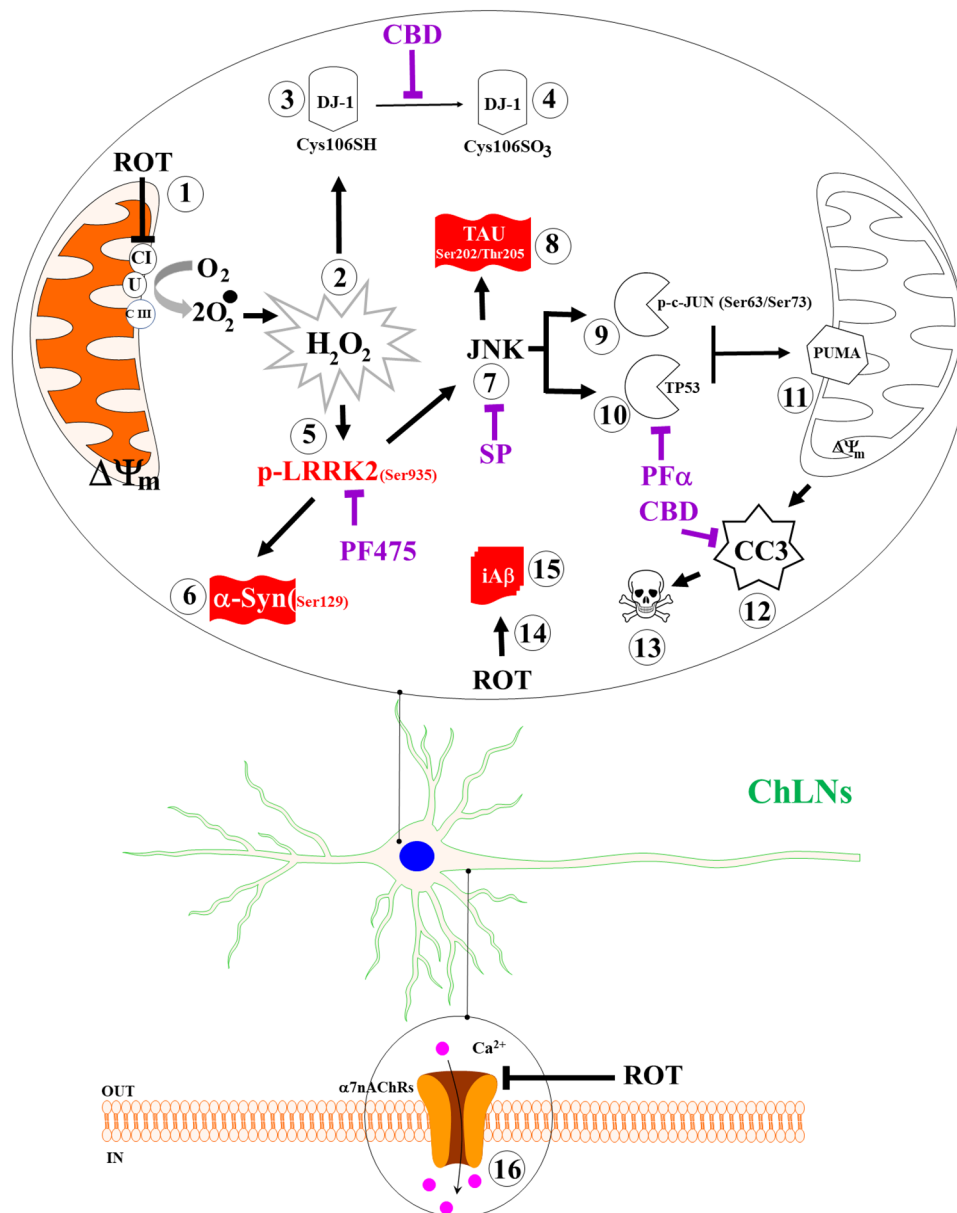


Fig. 9 Schematic model of the effect of rotenone (ROT) on Cholinergic-Like neurons (ChLNs): A mechanistic explanation of the interaction between ROT, LRRK2 kinase, α -synuclein, TAU, and β . Rotenone (ROT) binds to the ubiquinone binding site of mitochondrial complex I preventing electron transfer through flavin mononucleotide (FMN) to coenzyme Q10 (1). Interruption of the electron transport chain concomitantly generates anion superoxide ($O_2^{\cdot-}$) and hydrogen peroxide (H_2O_2 , 2). This last compound is capable of directly oxidized DJ-1Cys¹⁰⁶-SH (3) into DJ-1Cys¹⁰⁶-SO₃ (4), thereby disabling DJ-1 antioxidant signaling mechanisms. Alternatively, H_2O_2 activates LRRK 2 kinase (5) through activation of MEKK1/IKK or by autophosphorylation. Once LRRK 2 is phosphorylated at Ser⁹³⁵, the active kinase phosphorylates two major targets: (i) it phosphorylates α -Synuclein at Ser¹²⁹ residue (6), and (ii) indirectly activates JNK pathway (7). This last kinase in turn phosphorylates protein

TAU at Ser²⁰²/Tyr²⁰⁵ (8), activates via phosphorylation at Ser⁶³/Ser⁷³ pro-apoptotic c-JUN factor (9) and TP53 (10), which in turn transcribe PUMA (11), a BH-3-only Bcl-2 protein that induces mitochondria depolarization, resulting in cleaved caspase 3 (CC3, 12), which is responsible for chromatin condensation and DNA fragmentation (13), typical hallmarks of apoptosis. Additionally, ROT putatively binds to the PSEN1/ γ -secretase (14), impairing the process of Amyloid β Precursor Protein towards up-expression of internal accumulation of A β (iA β , 15) and to the α 7nAChRs (16), inducing Ca influx dysregulation in ChLNs. The coexistence of p-Ser¹²⁹ α -Syn (6), p-Ser²⁰²/Thr²⁰⁵ TAU (8), and iA β (15) constitute the pathological hallmark of PDD. Notably, selective inhibition of LRRK2, JNK, and TP 53 with PF475 (PF), SP600125 (SP), pifithrin- α (PFT), and cannabidiol (CBD) blunted the appearance of p- α -Syn (6), p-TAU (8), CC3 (12), condensed/ fragmented nuclei (13), and iA β (15)

Finally, we confirm that ROT-induced apoptosis involving mitochondria depolarization and activation of CASP3 (Li et al. 2003) reflected as CC3 in ChLNs. Indeed, ROT increased the expression of TP53 and PUMA. Interestingly, both transcription factors TP53 and p-c-JUN transcribed PUMA (Nakano and Vousden 2001; Yu et al. 2001; Lu et al. 2014), a BH-3-only proapoptotic protein directly involved in mitochondrial depolarization and apoptosis (Roufayel et al. 2022; Czabotar and Garcia-Saez 2023), thereby contributing to the release of apoptogenic cytochrome C and activation of CASP3 (Dorstyn et al. 2018). Taken together, these observations imply that mitochondrial up- and downstream signaling are critical to trigger apoptosis in ChLNs. This last assumption is further supported by significant reduction of apoptosis in ChLNs when co-treated with inhibitor TP53 pifithrin- α or LRRK2 inhibitor PF-06447475 and ROT.

Additionally, ROT almost abolishes the ACh-induced transient intracellular Ca^{2+} flux in ChLNs. This suggests that ROT, similar to extracellular (e) A β (Wang et al. 2000), somehow blocks the binding of ACh to ligand-gated Ca^{2+} ion channels (Uteshev 2012; Brown 2019). Moreover, docking analysis support the view that ROT can bind to nAChRs, e.g., $\alpha 7$ nAChR with high affinity (Table 1). These observations might explain why ROT impairs learning and memory in mice (Guo et al. 2022). However, further investigation is needed to clarify these issues. We conclude that ROT-induced apoptosis, co-existence of p- α -Syn, iA β , and p-TAU and neuronal Ca^{2+} influx dysfunction in ChLNs through OS-dependent and -independent mechanisms (Fig. 9).

For comparative purposes, we used PSEN 1 E280A (Soto-Mercado et al. 2020). Effectively, mutant ChLNs reproduced the pathological markers of Alzheimer's disease, involving iA β , p-TAU, and oxDJ-1. Additionally, mutant ChLNs showed loss of $\Delta\Psi_m$, up regulation of p-c-JUN, TP53, PUMA, and CC3, leading to apoptosis and eA β -induced Ca^{2+} influx impairments (Soto-Mercado et al. 2020). Therefore, ROT and iA β seem to be mechanistically homologous. Similar to ROT (this work), iA β disrupts mitochondria bioenergetics (Sinclair et al. 2021), thereby generating ROS/H $_2$ O $_2$, activates ASK-1 (Kadowaki et al. 2005), JNK/c-JUN axis, and p-TAU (Solas et al. 2023), and induces apoptosis dependent on CASP3 (Eimer and Vassar 2013). However, in contrast to ROT, A β selectively inhibit Complex IV (Canevari et al. 1999). Surprisingly, we found for the first time an important endogenously increase in p-Ser⁹³⁵ LRRK 2 and p-Ser¹²⁹ α -Syn in PSEN 1 E280A ChLNs compared to wild type ChLNs. Given that LRRK2 is an indispensable pro-apoptotic kinase (Quintero-Espinosa et al. 2017, 2023; Perez-Abshana et al. 2023), these results indicate that LRRK2 may play a major role in both DAergic and ChLNs demise. Furthermore, from

a neuropathologic perspective, our findings might explain why some brains from demented patients show a mixed pathology of dementia with Lewy bodies (DLB) and AD (Kantarci et al. 2020). We report for the first time that PSEN 1 E280A ChLNs display the typical p-Ser¹²⁹ α -Syn, a pathological feature found in PD, DLB, and PDD. However, whether p-Ser¹²⁹ α -Syn and p-Ser⁹³⁵ LRRK2 are positive markers in human brains from FAD PSEN 1 E280A patients need further investigation.

Here, we show that ChLNs derived from WJ-MSCs treated with ROT might be an excellent system to model PDD. Our findings have one major implication for PD and PDD. It is known that the most significant nonmotor symptom in PD is progressive cognitive impairment (Aarsland et al. 2021), and PDD may affect 80% of PD patients long-term (Russell et al. 2014). Unfortunately, this recognition has not translated into significant treatment advances. One possible explanation for this drawback is the lack of proper in vitro or in vivo models. Here, we provide an in vitro model that accounts for the molecular mechanism by which ROT-induced cell death occurs in ChLNs, the major neuronal group involved in early AD and late PD. Furthermore, we found that LRRK2 is a key master kinase that links both PD through p-Ser¹²⁹ α -Syn and FAD through apoptotic cell death signaling. This adds another layer of molecular complexity to the understanding of cell demise in both PD (Michel et al. 2016; Quintero-Espinosa et al. 2017, 2023; Velez-Pardo and Jimenez-Del-Rio 2020; Perez-Abshana et al. 2023) and FAD (Soto-Mercado et al. 2020; Brokaw et al. 2020). However, provided that LRRK2 is a druggable target (Thakur et al. 2022), it should be implemented in clinical trials including not only PDD but also PD as well as FAD patients. Our model system offers an understanding of the mechanisms of neurodegeneration in PD and AD. Nonetheless, our model has limitations. Although the data suggested that ROT impairs PSEN1 / γ -secretase towards increased accumulation of A β , there is no reasonable explanation for the endogenous production of iA β in PDD brains. It is worth mentioning that a reformulation of the amyloid cascade hypothesis (ACH), now known as ACH 2.0, provides enlightenment on this issue (Volloch and Rits-Volloch 2023). Accordingly, it is proposed that AD is triggered by a first benign stage, wherein an APP-derived iA β accumulated to sufficient levels in both sporadic (SAD) and FAD, and is driven by a second deleterious stage, wherein iA β generated dependently of APP in FAD and independently of APP in SAD induced mitochondrial dysfunction and apoptosis (Volloch and Rits-Volloch 2023). Therefore, the role of iA β and α -Syn pathology in the development of cognitive deficits in PD suggests that emerging disease-modifying therapies for AD may be beneficial for PDD patients.

Conclusion

We provide an *in vitro* model recreating the neuropathology of PDD induced by ROT in ChLNs. Indeed, ROT induces p- α -Syn, A β , p-Tau, and cell death in ChLNs. Furthermore, we identify the LRRK2 as master kinase that link both PD and AD via apoptotic cell death signaling. The “ChLNs plus ROT” approach provides an excellent platform to test for potential therapeutic strategies against PDD. Our data suggest that ROT induces a neuropathologic phenotype in ChLNs similar to that caused by the mutation PSEN1 E280A.

Supplementary Information The online version contains supplementary material available at <https://doi.org/10.1007/s12640-024-00705-3>.

Acknowledgements Not applicable

Author Contributions Conceptualization, C.V.-P, and M.J.-R.; methodology, D. G.-B., and M.M.-P.; formal analysis, D. G.-B., M.M.-P., and C.V.P; validation: D. G.-B. and M.M.-P.; investigation, C.V.-P., and M.J.-R.; resources, M.J.-R.; data curation, D. G.-B., and M.M.-P.; writing—original draft preparation, C.V.-P, and M.J.-R.; writing—review and editing, D. G.-B., M.M.-P.; C.V.-P., and M.J.-R.; supervision, M.M.-P., C.V.-P and M.J.-R.; project administration, C.V.-P and M.J.-R.; funding acquisition, M.J.-R. All authors have read and agreed to the published version of the manuscript.

Funding Open Access funding provided by Colombia Consortium This work was funded by MinCiencias (grant. no. 1115–807-62912, contract no. 749–2018).

Data Availability No datasets were generated or analysed during the current study.

Declarations

Ethical Approval Umbilical cord specimen donors supplied a signed informed consent approved by the ethics committee of the Sede de Investigación Universitaria (SIU), University of Antioquia, Medellín, Colombia (Act # 13–2015).

Human Ethics Not applicable.

Authors' Information D. G.-B. is a magister student of the Basic Biomedical Sciences Academic Corporation program at the Universidad de Antioquia (UdeA) funded by MinCiencias-Colombia. M.M.-P., C.V.-P. and M.J.-R. are associated and senior professors, respectively, at the University of Antioquia.

Consent to Participate Not applicable.

Consent for Publication Not applicable.

Competing Interest The authors declare no competing interests.

Open Access This article is licensed under a Creative Commons Attribution 4.0 International License, which permits use, sharing, adaptation, distribution and reproduction in any medium or format, as long

as you give appropriate credit to the original author(s) and the source, provide a link to the Creative Commons licence, and indicate if changes were made. The images or other third party material in this article are included in the article's Creative Commons licence, unless indicated otherwise in a credit line to the material. If material is not included in the article's Creative Commons licence and your intended use is not permitted by statutory regulation or exceeds the permitted use, you will need to obtain permission directly from the copyright holder. To view a copy of this licence, visit <http://creativecommons.org/licenses/by/4.0/>.

References

- Aarsland D, Batzu L, Halliday GM et al (2021) Parkinson disease-associated cognitive impairment. *Nat Rev Dis Primers* 7:47. <https://doi.org/10.1038/s41572-021-00280-3>
- Abrishamdar M, Jalali MS, Farbood Y (2023) Targeting Mitochondria as a Therapeutic Approach for Parkinson's Disease. *Cell Mol Neurobiol* 43:1499–1518. <https://doi.org/10.1007/s10571-022-01265-w>
- Adan A, Alizada G, Kiraz Y et al (2017) Flow cytometry: basic principles and applications. *Crit Rev Biotechnol* 37:163–176. <https://doi.org/10.3109/07388551.2015.1128876>
- Andrade S, Nunes D, Dabur M et al (2023) Therapeutic Potential of Natural Compounds in Neurodegenerative Diseases: Insights from Clinical Trials. *Pharmaceutics* 15:212. <https://doi.org/10.3390/pharmaceutics15010212>
- Antunes F, Brito PM (2017) Quantitative biology of hydrogen peroxide signaling. *Redox Biol* 13:1–7. <https://doi.org/10.1016/j.redox.2017.04.039>
- Bai XC, Rajendra E, Yang G, Shi Y, Scheres SH (2015) Sampling the conformational space of the catalytic subunit of human γ -secretase. *Elife* 4:e11182. <https://doi.org/10.7554/eLife.11182>
- Biosa A, Sandrelli F, Beltramini M et al (2017) Recent findings on the physiological function of DJ-1: Beyond Parkinson's disease. *Neurobiol Dis* 108:65–72. <https://doi.org/10.1016/j.nbd.2017.08.005>
- Bloem BR, Okun MS, Klein C (2021) Parkinson's disease. *The Lancet* 397:2284–2303. [https://doi.org/10.1016/S0140-6736\(21\)00218-X](https://doi.org/10.1016/S0140-6736(21)00218-X)
- Brokaw DL, Piras IS, Mastroeni D et al (2020) Cell death and survival pathways in Alzheimer's disease: an integrative hypothesis testing approach utilizing -omic data sets. *Neurobiol Aging* 95:15–25. <https://doi.org/10.1016/j.neurobiolaging.2020.06.022>
- Brown DA (2019) Acetylcholine and cholinergic receptors. *Brain Neurosci Adv* 3:239821281882050. <https://doi.org/10.1177/2398212818820506>
- Canevari L, Clark JB, Bates TE (1999) β -Amyloid fragment 25–35 selectively decreases complex IV activity in isolated mitochondria. *FEBS Lett* 457:131–134. [https://doi.org/10.1016/S0014-5793\(99\)01028-5](https://doi.org/10.1016/S0014-5793(99)01028-5)
- Castillo-Arellano J, Canseco-Alba A, Cutler SJ, León F (2023) The Polypharmacological Effects of Cannabidiol. *Molecules* 28:3271. <https://doi.org/10.3390/molecules28073271>
- Chaves RS, Melo TQ, Martins SA, Ferrari MF (2010) Protein aggregation containing beta-amyloid, alpha-synuclein and hyperphosphorylated tau in cultured cells of hippocampus, substantia nigra and locus coeruleus after rotenone exposure. *BMC Neurosci* 11:144. <https://doi.org/10.1186/1471-2202-11-144>
- Chaves RS, Kazi AI, Silva CM et al (2016) Presence of insoluble Tau following rotenone exposure ameliorates basic pathways

- associated with neurodegeneration. *IBRO Rep* 1:32–45. <https://doi.org/10.1016/j.ibror.2016.09.001>
- Czabotar PE, Garcia-Saez AJ (2023) Mechanisms of BCL-2 family proteins in mitochondrial apoptosis. *Nat Rev Mol Cell Biol* 24:732–748. <https://doi.org/10.1038/s41580-023-00629-4>
- Despres C, Byrne C, Qi H et al (2017) Identification of the Tau phosphorylation pattern that drives its aggregation. *Proc Natl Acad Sci* 114:9080–9085. <https://doi.org/10.1073/pnas.1708448114>
- Deutch AY, Roth RH (2014) Pharmacology and Biochemistry of Synaptic Transmission. Introduction to Cellular and Molecular Neuroscience. <https://doi.org/10.1016/B978-0-12-397179-1.00007-5>
- Di Marzo N, Chisci E, Giovannoni R (2018) The Role of Hydrogen Peroxide in Redox-Dependent Signaling: Homeostatic and Pathological Responses in Mammalian Cells. *Cells* 7:156. <https://doi.org/10.3390/cells7100156>
- Dickson DW (2012) Parkinson's Disease and Parkinsonism: Neuropathology. *Cold Spring Harb Perspect Med* 2:a009258–a009258. <https://doi.org/10.1101/cshperspect.a009258>
- Do HN, Devkota S, Bhattarai A et al (2023) Effects of presenilin-1 familial Alzheimer's disease mutations on γ -secretase activation for cleavage of amyloid precursor protein. *Commun Biol* 6:174. <https://doi.org/10.1038/s42003-023-04539-1>
- Dominici M, Le Blanc K, Mueller I et al (2006) Minimal criteria for defining multipotent mesenchymal stromal cells. The International Society for Cellular Therapy position statement. *Cytotherapy* 8:315–317. <https://doi.org/10.1080/14653240600855905>
- Dong-Chen X, Yong C, Yang X et al (2023) Signaling pathways in Parkinson's disease: molecular mechanisms and therapeutic interventions. *Signal Transduct Target Ther* 8:73. <https://doi.org/10.1038/s41392-023-01353-3>
- Dorstyn L, Akey CW, Kumar S (2018) New insights into apoptosome structure and function. *Cell Death Differ* 25:1194–1208. <https://doi.org/10.1038/s41418-017-0025-z>
- Du T, Wang L, Liu W et al (2021) Biomarkers and the Role of α -Synuclein in Parkinson's Disease. *Front Aging Neurosci* 13:645996. <https://doi.org/10.3389/fnagi.2021.645996>
- Dzambo N, Inesta-Vaquera F, Zhang J et al (2012) The IkappaB Kinase Family Phosphorylates the Parkinson's Disease Kinase LRRK2 at Ser935 and Ser910 during Toll-Like Receptor Signaling. *PLoS ONE* 7:e39132. <https://doi.org/10.1371/journal.pone.0039132>
- Eimer WA, Vassar R (2013) Neuron loss in the 5XFAD mouse model of Alzheimer's disease correlates with intraneuronal A β 42 accumulation and Caspase-3 activation. *Mol Neurodegener* 8:2. <https://doi.org/10.1186/1750-1326-8-2>
- Fang N, Casida JE (1999) Cubé Resin Insecticide: Identification and Biological Activity of 29 Rotenoid Constituents. *J Agric Food Chem* 47:2130–2136. <https://doi.org/10.1021/jf981188x>
- Ferreira-Junior NC, Campos AC, Guimarães FS et al (2020) Biological bases for a possible effect of cannabidiol in Parkinson's disease. *Braz J Psychiatry* 42:218–224. <https://doi.org/10.1590/1516-4446-2019-0460>
- Fujiwara H, Hasegawa M, Dohmae N et al (2002) α -Synuclein is phosphorylated in synucleinopathy lesions. *Nat Cell Biol* 4:160–164. <https://doi.org/10.1038/ncb748>
- Giguère N, Burke Nanni S, Trudeau L-E (2018) On Cell Loss and Selective Vulnerability of Neuronal Populations in Parkinson's Disease. *Front Neurol* 9:455. <https://doi.org/10.3389/fneur.2018.00455>
- Goetz CG, Emre M, Dubois B (2009) Parkinson's disease dementia: Definitions, guidelines, and research perspectives in diagnosis. *Ann Neurol* 64:S81–S92. <https://doi.org/10.1002/ana.21455>
- Golde TE (2009) The therapeutic importance of understanding mechanisms of neuronal cell death in neurodegenerative disease. *Mol Neurodegener* 4:8. <https://doi.org/10.1186/1750-1326-4-8>
- Guo Z, Ruan Z, Zhang D et al (2022) Rotenone impairs learning and memory in mice through microglia-mediated blood brain barrier disruption and neuronal apoptosis. *Chemosphere* 291:132982. <https://doi.org/10.1016/j.chemosphere.2021.132982>
- Hacke ACM, Lima D, De Costa F et al (2019) Probing the antioxidant activity of Δ 9-tetrahydrocannabinol and cannabidiol in Cannabis sativa extracts. *Analyst* 144:4952–4961. <https://doi.org/10.1039/c9an00890j>
- Hamm M, Bailey R, Shaw G et al (2015) Physiologically relevant factors influence tau phosphorylation by leucine-rich repeat kinase 2. *J Neurosci Res* 93:1567–1580. <https://doi.org/10.1002/jnr.23614>
- Han J, Fan Y, Wu P et al (2021) Parkinson's Disease Dementia: Synergistic Effects of Alpha-Synuclein, Tau, Beta-Amyloid, and Iron. *Front Aging Neurosci* 13:743754. <https://doi.org/10.3389/fnagi.2021.743754>
- Hepp Rehfeldt SC, Majolo F, Goettert MI, Laufer S (2020) c-Jun N-Terminal Kinase Inhibitors as Potential Leads for New Therapeutics for Alzheimer's Diseases. *Int J Mol Sci* 21:9677. <https://doi.org/10.3390/ijms21249677>
- Höglinger GU, Lannuzel A, Khondiker ME et al (2005) The mitochondrial complex I inhibitor rotenone triggers a cerebral tauopathy. *J Neurochem* 95:930–939. <https://doi.org/10.1111/j.1471-4159.2005.03493.x>
- Hyde LA, Zhang Q, Del Vecchio RA et al (2013) In Vivo Characterization of a Novel γ -Secretase Inhibitor SCH 697466 in Rodents and Investigation of Strategies for Managing Notch-Related Side Effects. *Int J Alzheimers Dis* 2013:1–14. <https://doi.org/10.1155/2013/823528>
- Irwin DJ, Lee VM-Y, Trojanowski JQ (2013) Parkinson's disease dementia: convergence of α -synuclein, tau and amyloid- β pathologies. *Nat Rev Neurosci* 14:626–636. <https://doi.org/10.1038/nrn3549>
- Jankovic J (2008) Parkinson's disease: clinical features and diagnosis. *J Neurol Neurosurg Psychiatry* 79:368–376. <https://doi.org/10.1136/jnnp.2007.131045>
- Jellinger KA (2023) Morphological characteristics differentiate dementia with Lewy bodies from Parkinson disease with and without dementia. *J Neural Transm* 130:891–904. <https://doi.org/10.1007/s00702-023-02660-3>
- Kadowaki H, Nishitoh H, Urano F et al (2005) Amyloid β induces neuronal cell death through ROS-mediated ASK1 activation. *Cell Death Differ* 12:19–24. <https://doi.org/10.1038/sj.cdd.4401528>
- Kamikawaji S, Ito G, Iwatsubo T (2009) Identification of the Autophosphorylation Sites of LRRK2. *Biochemistry* 48:10963–10975. <https://doi.org/10.1021/bi9011379>
- Kantarci K, Lowe VJ, Chen Q et al (2020) β -Amyloid PET and neuropathology in dementia with Lewy bodies. *Neurology* 94:e282–e291. <https://doi.org/10.1212/WNL.0000000000008818>
- Ke M, Chong C-M, Zhu Q et al (2021) Comprehensive Perspectives on Experimental Models for Parkinson's Disease. *Aging Dis* 12:223. <https://doi.org/10.14336/AD.2020.0331>
- Kim JR (2023) Oligomerization by co-assembly of β -amyloid and α -synuclein. *Front Mol Biosci* 10:1153839. <https://doi.org/10.3389/fmolb.2023.1153839>
- Kinumi T, Kimata J, Taira T et al (2004) Cysteine-106 of DJ-1 is the most sensitive cysteine residue to hydrogen peroxide-mediated oxidation in vivo in human umbilical vein endothelial cells. *Biochem Biophys Res Commun* 317:722–728. <https://doi.org/10.1016/j.bbrc.2004.03.110>
- Knopman DS, Amieva H, Petersen RC et al (2021) Alzheimer Disease. *Nat Rev Dis Primers* 7:33. <https://doi.org/10.1038/s41572-021-00269-y>
- Kouli A, Camacho M, Allinson K, Williams-Gray CH (2020) Neuroinflammation and protein pathology in Parkinson's disease dementia. *Acta Neuropathol Commun* 8:211. <https://doi.org/10.1186/s40478-020-01083-5>

- Lawana V, Cannon JR (2020) Rotenone neurotoxicity: Relevance to Parkinson's disease. *Adv Neurotoxicol* 4:209–254. <https://doi.org/10.1016/bs.ant.2019.11.004>
- Lazic SE, Clarke-Williams CJ, Munafò MR (2018) What exactly is 'N' in cell culture and animal experiments? *PLoS Biol* 16:e2005282. <https://doi.org/10.1371/journal.pbio.2005282>
- Lee J, Song L, Terracina G et al (2011) Identification of Presenilin 1-Selective γ -Secretase Inhibitors with Reconstituted γ -Secretase Complexes. *Biochemistry* 50:4973–4980. <https://doi.org/10.1021/bi200026m>
- Li N, Ragheb K, Lawler G et al (2003) Mitochondrial Complex I Inhibitor Rotenone Induces Apoptosis through Enhancing Mitochondrial Reactive Oxygen Species Production. *J Biol Chem* 278:8516–8525. <https://doi.org/10.1074/jbc.M210432200>
- Li X, Moore DJ, Xiong Y et al (2010) Reevaluation of Phosphorylation Sites in the Parkinson Disease-associated Leucine-rich Repeat Kinase 2. *J Biol Chem* 285:29569–29576. <https://doi.org/10.1074/jbc.M110.127639>
- Lichtman JW, Conchello J-A (2005) Fluorescence microscopy. *Nat Methods* 2:910–919. <https://doi.org/10.1038/nmeth817>
- Liu AKL, Chang RC-C, Pearce RKB, Gentleman SM (2015) Nucleus basalis of Meynert revisited: anatomy, history and differential involvement in Alzheimer's and Parkinson's disease. *Acta Neuropathol* 129:527–540. <https://doi.org/10.1007/s00401-015-1392-5>
- Liu AKL, Chau TW, Lim EJ et al (2019) Hippocampal CA2 Lewy pathology is associated with cholinergic degeneration in Parkinson's disease with cognitive decline. *Acta Neuropathol Commun* 7:61. <https://doi.org/10.1186/s40478-019-0717-3>
- Liu Y, Yang X, Gan J et al (2022) CB-Dock2: improved protein–ligand blind docking by integrating cavity detection, docking and homologous template fitting. *Nucleic Acids Res* 50:W159–W164. <https://doi.org/10.1093/nar/gkac394>
- Lu H, Hou G, Zhang Y et al (2014) c-Jun transactivates Puma gene expression to promote osteoarthritis. *Mol Med Rep* 9:1606–1612. <https://doi.org/10.3892/mmr.2014.1981>
- Macdonald R, Barnes K, Hastings C, Mortiboys H (2018) Mitochondrial abnormalities in Parkinson's disease and Alzheimer's disease: can mitochondria be targeted therapeutically? *Biochem Soc Trans* 46:891–909. <https://doi.org/10.1042/BST20170501>
- Mailloux RJ (2015) Teaching the fundamentals of electron transfer reactions in mitochondria and the production and detection of reactive oxygen species. *Redox Biol* 4:381–398. <https://doi.org/10.1016/j.redox.2015.02.001>
- Maler JM, Klafki H-W, Paul S et al (2007) Urea-based two-dimensional electrophoresis of beta-amyloid peptides in human plasma: Evidence for novel A β species. *Proteomics* 7:3815–3820. <https://doi.org/10.1002/pmic.200700311>
- Marinho HS, Real C, Cyrne L et al (2014) Hydrogen peroxide sensing, signaling and regulation of transcription factors. *Redox Biol* 2:535–562. <https://doi.org/10.1016/j.redox.2014.02.006>
- Mendivil-Perez M, Velez-Pardo C, Jimenez-Del-Rio M (2016) Neuroprotective Effect of the LRRK2 Kinase Inhibitor PF-06447475 in Human Nerve-Like Differentiated Cells Exposed to Oxidative Stress Stimuli: Implications for Parkinson's Disease. *Neurochem Res* 41:2675–2692. <https://doi.org/10.1007/s11064-016-1982-1>
- Mendivil-Perez M, Velez-Pardo C, Jimenez-Del-Rio M (2019) Direct transdifferentiation of human Wharton's jelly mesenchymal stromal cells into cholinergic-like neurons. *J Neurosci Methods* 312:126–138. <https://doi.org/10.1016/j.jneumeth.2018.11.019>
- Mendivil-Perez M, Felizardo-Otalvaro AA, Jimenez-Del-Rio M, Velez-Pardo C (2023) Cannabidiol Protects Dopaminergic-like Neurons against Paraquat- and Maneb-Induced Cell Death through Safeguarding DJ-1/CYS¹⁰⁶ and Caspase 3 Independently of Cannabinoid Receptors: Relevance in Parkinson's Disease. *ACS Chem Neurosci* 14:2159–2171. <https://doi.org/10.1021/acscchemneuro.3c00176>
- Michel PP, Hirsch EC, Hunot S (2016) Understanding Dopaminergic Cell Death Pathways in Parkinson Disease. *Neuron* 90:675–691. <https://doi.org/10.1016/j.neuron.2016.03.038>
- Nadeau PJ, Charette SJ, Landry J (2009) REDOX Reaction at ASK1-Cys250 Is Essential for Activation of JNK and Induction of Apoptosis. *Mol Biol Cell* 20:3628–3637. <https://doi.org/10.1091/mbc.e09-03-0211>
- Nakano K, Vousden KH (2001) PUMA, a Novel Proapoptotic Gene, Is Induced by p53. *Mol Cell* 7:683–694. [https://doi.org/10.1016/S1097-2765\(01\)00214-3](https://doi.org/10.1016/S1097-2765(01)00214-3)
- Neddens J, Temmel M, Flunkert S et al (2018) Phosphorylation of different tau sites during progression of Alzheimer's disease. *Acta Neuropathol Commun* 6:52. <https://doi.org/10.1186/s40478-018-0557-6>
- Neves M, Grãos M, Anjo SI, Manadas B (2022) Modulation of signaling pathways by DJ-1: An updated overview. *Redox Biol* 51:102283. <https://doi.org/10.1016/j.redox.2022.102283>
- Noviello CM, Gharpure A, Mukhtasimova N et al (2021) Structure and gating mechanism of the $\alpha 7$ nicotinic acetylcholine receptor. *Cell* 184:2121–2134.e13. <https://doi.org/10.1016/j.cell.2021.02.049>
- Pap P, Kőszeghy Á, Szűcs G, Rusznák Z (2009) Cytoplasmic Ca²⁺ concentration changes evoked by cholinergic stimulation in primary astrocyte cultures prepared from the rat cochlear nucleus. *Hear Res* 255:73–83. <https://doi.org/10.1016/j.heares.2009.05.006>
- Pepou G, Grazia Giovannini M (2017) The fate of the brain cholinergic neurons in neurodegenerative diseases. *Brain Res* 1670:173–184. <https://doi.org/10.1016/j.brainres.2017.06.023>
- Perez-Abshana LP, Mendivil-Perez M, Velez-Pardo C, Jimenez-Del-Rio M (2023) Rotenone Blocks the Glucocerebrosidase Enzyme and Induces the Accumulation of Lysosomes and Autophagolysosomes Independently of LRRK2 Kinase in HEK-293 Cells. *Int J Mol Sci* 24:10589. <https://doi.org/10.3390/ijms241310589>
- Phillips O, Ghosh D, Fernandez HH (2023) Parkinson Disease Dementia Management: an Update of Current Evidence and Future Directions. *Curr Treat Options Neurol* 25:93–119. <https://doi.org/10.1007/s11940-023-00749-4>
- Qing H, Wong W, McGeer EG, McGeer PL (2009) Lrrk2 phosphorylates alpha synuclein at serine 129: Parkinson disease implications. *Biochem Biophys Res Commun* 387:149–152. <https://doi.org/10.1016/j.bbrc.2009.06.142>
- Quintero-Espinosa D, Jimenez-Del-Rio M, Velez-Pardo C (2017) Knockdown transgenic Lrrk Drosophila resists paraquat-induced locomotor impairment and neurodegeneration: A therapeutic strategy for Parkinson's disease. *Brain Res* 1657:253–261. <https://doi.org/10.1016/j.brainres.2016.12.023>
- Quintero-Espinosa DA, Sanchez-Hernandez S, Velez-Pardo C et al (2023) LRRK2 Knockout Confers Resistance in HEK-293 Cells to Rotenone-Induced Oxidative Stress, Mitochondrial Damage, and Apoptosis. *Int J Mol Sci* 24:10474. <https://doi.org/10.3390/ijms241310474>
- Read AD, Bentley RET, Archer SL, Dunham-Snary KJ (2021) Mitochondrial iron–sulfur clusters: Structure, function, and an emerging role in vascular biology. *Redox Biol* 47:102164. <https://doi.org/10.1016/j.redox.2021.102164>
- Ren Y, Liu W, Jiang H et al (2005) Selective Vulnerability of Dopaminergic Neurons to Microtubule Depolymerization. *J Biol Chem* 280:34105–34112. <https://doi.org/10.1074/jbc.M503483200>
- Repici M, Giorgini F (2019) DJ-1 in Parkinson's Disease: Clinical Insights and Therapeutic Perspectives. *J Clin Med* 8:1377. <https://doi.org/10.3390/jcm8091377>
- Reynolds CH, Betts JC, Blackstock WP et al (2000) Phosphorylation Sites on Tau Identified by Nano-electrospray Mass Spectrometry. *J Neurochem* 74:1587–1595. <https://doi.org/10.1046/j.1471-4159.2000.0741587.x>

- Roufayel R, Younes K, Al-Sabi A, Murshid N (2022) BH3-Only Proteins Noxa and Puma Are Key Regulators of Induced Apoptosis. *Life* 12:256. <https://doi.org/10.3390/life12020256>
- Russell A, Drozdova A, Wang W, Thomas M (2014) The Impact of Dementia Development Concurrent with Parkinson's Disease: A New Perspective. *CNS Neurol Disord Drug Targets* 13:1160–1168
- Sae-Yun A, Ovatarnporn C, Itharat A, Wiwattanapatee R (2006) Extraction of rotenone from *Derris elliptica* and *Derris malaccensis* by pressurized liquid extraction compared with maceration. *J Chromatogr A* 1125:172–176. <https://doi.org/10.1016/j.chroma.2006.05.075>
- Saito Y (2017) DJ-1 as a Biomarker of Parkinson's Disease. *Adv Exp Med Biol* 1037:149–171. https://doi.org/10.1007/978-981-10-6583-5_10
- Schiller J, Zickermann V (2022) Binding of Natural Inhibitors to Respiratory Complex I. *Pharmaceuticals* 15:1088. <https://doi.org/10.3390/ph15091088>
- Sekiguchi-Tonosaki M, Obata M, Haruki A et al (2009) Acetylcholine induces Ca²⁺ signaling in chicken retinal pigmented epithelial cells during differentiation. *Am J Physiol-Cell Phys* 296:C1195–C1206. <https://doi.org/10.1152/ajpcell.00423.2008>
- Serneels L, Narlawar R, Perez-Benito L et al (2023) Selective inhibitors of the PSEN1-gamma-secretase complex. *J Biol Chem* 299(6):104794. <https://doi.org/10.1016/j.jbc.2023.104794>
- Shanley MR, Hawley D, Leung S et al (2015) LRRK2 Facilitates tau Phosphorylation through Strong Interaction with tau and cdk5. *Biochemistry* 54:5198–5208. <https://doi.org/10.1021/acs.biochem.5b00326>
- Sinclair P, Baranova A, Kabbani N (2021) Mitochondrial Disruption by Amyloid Beta 42 Identified by Proteomics and Pathway Mapping. *Cells* 10:2380. <https://doi.org/10.3390/cells10092380>
- Singh S, Agrawal N, Goyal A (2024) Role of Alpha-7-Nicotinic Acetylcholine Receptor in Alzheimer's Disease. *CNS Neurol Disord Drug Targets* 23:384–394. <https://doi.org/10.2174/1871527322666230627123426>
- Smith C, Malek N, Grosset K et al (2019) Neuropathology of dementia in patients with Parkinson's disease: a systematic review of autopsy studies. *J Neurol Neurosurg Psychiatry* 90:1234–1243. <https://doi.org/10.1136/jnnp-2019-321111>
- Sogorb-Esteve A, García-Ayllón M-S, Llansola M et al (2018) Inhibition of γ -Secretase Leads to an Increase in Presenilin-1. *Mol Neurobiol* 55:5047–5058. <https://doi.org/10.1007/s12035-017-0705-1>
- Solas M, Vela S, Smerdov C et al (2023) JNK Activation in Alzheimer's Disease Is Driven by Amyloid β and Is Associated with Tau Pathology. *ACS Chem Neurosci* 14:1524–1534. <https://doi.org/10.1021/acschemneuro.3c00093>
- Soto-Mercado V, Mendivil-Perez M, Velez-Pardo C et al (2020) Cholinergic-like neurons carrying PSEN1 E280A mutation from familial Alzheimer's disease reveal intraneuronal sAPP β fragments accumulation, hyperphosphorylation of TAU, oxidative stress, apoptosis and Ca²⁺ dysregulation: Therapeutic implications. *PLoS ONE* 15:e0221669. <https://doi.org/10.1371/journal.pone.0221669>
- Srivastava P, Panda D (2007) Rotenone inhibits mammalian cell proliferation by inhibiting microtubule assembly through tubulin binding. *FEBS J* 274:4788–4801. <https://doi.org/10.1111/j.1742-4658.2007.06004.x>
- Svedružić ŽM, Šendula Jengiđ V, Ostojić L (2023) The Binding of Different Substrate Molecules at the Docking Site and the Active Site of γ -Secretase Can Trigger Toxic Events in Sporadic and Familial Alzheimer's Disease. *Int J Mol Sci* 24:1835. <https://doi.org/10.3390/ijms24031835>
- Takeyama N, Miki S, Hirakawa A, Tanaka T (2002) Role of the Mitochondrial Permeability Transition and Cytochrome c Release in Hydrogen Peroxide-Induced Apoptosis. *Exp Cell Res* 274:16–24. <https://doi.org/10.1006/excr.2001.5447>
- Thakur G, Kumar V, Lee KW, Won C (2022) Structural Insights and Development of LRRK2 Inhibitors for Parkinson's Disease in the Last Decade. *Genes (basel)* 13:1426. <https://doi.org/10.3390/genes13081426>
- Ullrich C, Humpel C (2009) Rotenone Induces Cell Death of Cholinergic Neurons in an Organotypic Co-Culture Brain Slice Model. *Neurochem Res* 34:2147–2153. <https://doi.org/10.1007/s11064-009-0014-9>
- Usmani A, Shavarebi F, Hiniker A (2021) The Cell Biology of LRRK2 in Parkinson's Disease. *Mol Cell Biol* 41:e00660-e720. <https://doi.org/10.1128/MCB.00660-20>
- Uteshev VV (2012) α 7 Nicotinic ACh Receptors as a Ligand-Gated Source of Ca²⁺ Ions: The Search for a Ca²⁺ Optimum. *Adv Exp Med Biol* 740:603–638. https://doi.org/10.1007/978-94-007-2888-2_27
- Vasconcellos LFR, Pereira JS (2015) Parkinson's disease dementia: Diagnostic criteria and risk factor review. *J Clin Exp Neuropsychol* 37:988–993. <https://doi.org/10.1080/13803395.2015.1073227>
- Velez-Pardo C, Garcia Ospina G, Jimenez del Rio M (2002) A β [25–35] Peptide and Iron Promote Apoptosis in Lymphocytes by an Oxidative Stress Mechanism: Involvement of H₂O₂, Caspase-3, NF- κ B, p53 and c-Jun. *Neurotoxicology* 23:351–365. [https://doi.org/10.1016/S0161-813X\(02\)00081-5](https://doi.org/10.1016/S0161-813X(02)00081-5)
- Velez-Pardo C, Jimenez-Del-Rio M (2020) Oxidative stress signaling and regulated cell death in Parkinson's disease. In *Genetics, Neurology, Behavior, and Diet in Parkinson's Disease*. *Neurosci Parkinson* 2:157–173. <https://doi.org/10.1016/B978-0-12-815950-7.00010-2>
- Viswanathan S, Shi Y, Galipeau J et al (2019) Mesenchymal stem versus stromal cells: International Society for Cell & Gene Therapy (ISCT®) Mesenchymal Stromal Cell committee position statement on nomenclature. *Cytotherapy* 21:1019–1024. <https://doi.org/10.1016/j.jcyt.2019.08.002>
- Volloch V, Rits-Volloch S (2023) The Amyloid Cascade Hypothesis 2.0: Generalization of the Concept. *J Alzheimers Dis Rep* 7:21–35. <https://doi.org/10.3233/ADR-220079>
- Wang H-Y, Lee DHS, D'Andrea MR et al (2000) β -Amyloid1–42 Binds to α 7 Nicotinic Acetylcholine Receptor with High Affinity. *J Biol Chem* 275:5626–5632. <https://doi.org/10.1074/jbc.275.8.5626>
- Ward JM, Cockcroft VB, Lunt GG et al (1990) Methyllycaconitine: a selective probe for neuronal α -bungarotoxin binding sites. *FEBS Lett* 270:45–48. [https://doi.org/10.1016/0014-5793\(90\)81231-C](https://doi.org/10.1016/0014-5793(90)81231-C)
- West AB, Moore DJ, Choi C et al (2007) Parkinson's disease-associated mutations in LRRK2 link enhanced GTP-binding and kinase activities to neuronal toxicity. *Hum Mol Genet* 16:223–232. <https://doi.org/10.1093/hmg/ddl471>
- Wiltfang J, Esselmann H, Cupers P et al (2001) Elevation of β -Amyloid Peptide 2–42 in Sporadic and Familial Alzheimer's Disease and Its Generation in PS1 Knockout Cells. *J Biol Chem* 276:42645–42657. <https://doi.org/10.1074/jbc.M102790200>
- Wu W-L, Domalski M, Burnett DA et al (2012) Discovery of SCH 900229, a Potent Presenilin 1 Selective γ -Secretase Inhibitor for the Treatment of Alzheimer's Disease. *ACS Med Chem Lett* 3:892–896. <https://doi.org/10.1021/ml300044f>
- Xia W (2019) γ -Secretase and its modulators: Twenty years and beyond. *Neurosci Lett* 701:162–169. <https://doi.org/10.1016/j.neulet.2019.02.011>
- Xia Y, Prokop S, Gorion K-MM et al (2020) Tau Ser208 phosphorylation promotes aggregation and reveals neuropathologic diversity in Alzheimer's disease and other tauopathies. *Acta Neuropathol Commun* 8:88. <https://doi.org/10.1186/s40478-020-00967-w>
- Yu J, Zhang L, Hwang PM et al (2001) PUMA Induces the Rapid Apoptosis of Colorectal Cancer Cells. *Mol Cell* 7:673–682. [https://doi.org/10.1016/S1097-2765\(01\)00213-1](https://doi.org/10.1016/S1097-2765(01)00213-1)
- Zhang P, Zhang M, Mellich TA et al (2022a) Variation in Rotenone and Deguelin Contents among Strains across Four Tephrosia

- Species and Their Activities against Aphids and Whiteflies. *Toxins (basel)* 14:339. <https://doi.org/10.3390/toxins14050339>
- Zhang X-B, Li J, Gu J, Zeng Y-Q (2022b) Roles of Cannabidiol in the Treatment and Prevention of Alzheimer's Disease by Multi-target Actions. *Mini-Reviews in Med Chem* 22:43–51. <https://doi.org/10.2174/1389557521666210331162857>
- Zhu Y, Shuai W, Zhao M et al (2022) Unraveling the Design and Discovery of c-Jun N-Terminal Kinase Inhibitors and Their Therapeutic Potential in Human Diseases. *J Med Chem* 65:3758–3775. <https://doi.org/10.1021/acs.jmedchem.1c01947>
- Zubairi SI, Sarmidi MR, Aziz RA (2014) A Study of Rotenone from Derris Roots of Varies Location, Plant Parts and Types of Solvent Used. *Adv Environ Biol* 8:445–449

Publisher's Note Springer Nature remains neutral with regard to jurisdictional claims in published maps and institutional affiliations.